RESEARCH MEMORANDUM

CALCULATIVE METHOD FOR ESTIMATING THE INTERFERENCE PRESSURE FIELD AT ZERO LIFT ON A SYMMETRICAL SWEPT-BACK WING MOUNTED ON A CIRCULAR CYLINDRICAL BODY

By Jack N. Nielsen and Frederick H. Matteson

Ames Aeronautical Laboratory
Moffett Field, Calif.

NATIONAL ADVISORY COMMITTEE
FOR AERONAUTICS

WASHINGTON
August 5, 1949

NACA RM A9E19

NATIONAL ADVISORY COMMITTEE FOR AERONAUTICS

RESEARCH MEMORANDUM

CALCULATIVE METHOD FOR ESTIMATING THE INTERFERENCE PRESSURE FIELD AT ZERO LIFT ON A SYMMETRICAL SWEPT-BACK WING MOUNTED ON A CIRCULAR CYLINDRICAL BODY

By Jack N. Nielsen and Frederick H. Matteson

SUMMARY

An approximate method is presented for calculating the interference pressure distribution at zero lift of a symmetrical swept-back wing mounted on a circular cylindrical body with the chord plane of the wing passing through the axis of the body. The method employed is based on linear theory and is an approximate first-order method. An example illustrating the method is presented for a wing-body combination consisting of a circular cylindrical body and an untapered wing swept back 60°. The wing considered in the example has a double-wedge section with the maximum thickness at the midchord, a chord equal to twice the body diameter, and a spanwise distance from the wing-body juncture to the wing tip of two body diameters. The effects of a body nose on the wing pressure distribution are not considered in determining the pressure drag of the wing in combination. It is found that the pressure drag of the wing in combination is less than that of the two exposed half-wings joined together.

INTRODUCTION

At subsonic speeds, wing-body interference has important effects on the aerodynamic characteristics of an airplane. At supersonic speeds, wing-body interference assumes even greater importance because of the relatively large bodies and small wings usually specified for aircraft designed for flight at such speeds. Swept-back wings probably have greater interference effects at supersonic speeds than unswept or swept-forward wings because greater areas of swept-back wings lie within the region of influence of the wing-body juncture.

Past work on wing-body interference at supersonic speeds has been

largely confined to lift and moment interference. Using the concepts developed by R. T. Jones in his low-aspect-ratio, triangular-wing theory (reference 1), Spreiter (reference 2) has determined the effect of a pointed, slender body of revolution on the lift-curve slope and center-of-pressure location of a wing-body configuration. Browne, Friedman, and Hodes (reference 3), using the methods of conical supersonic flow, have determined the loading on a triangular-wing conical-body combination with a common apex. Ferrari (reference 4) has analyzed the lift and moment interference between a flat rectangular lifting surface and a pointed body of revolution.

There has been little work on the effects of wing thickness on the interference pressure distributions of wing-body combinations at supersonic speeds. It is the purpose of this report to present an approximate calculative method for determining the pressure field due to interaction between a wing with a double-wedge section that is swept behind the Mach cone and the circular cylindrical portion of the body of revolution in which it is mounted. The combination is analyzed at zero angle of attack with the chord plane of the wing passing through the body axis. The interference pressure distributions, acting at several spanwise positions of the wing in combination, are given in the report together with the wing interference pressure drag.

The emphasis in the analysis is placed on swept-back wings, the surfaces of which are composed of planes. The entire analysis, based on the linearized theory of supersonic flow, is for a free-stream Mach number of $\sqrt{2}$. The method for applying the results of the analysis to other Mach numbers is given at the end of the text. The approximate nature of the solution arises from the mathematical complexity of the complete interference problem. One of the components of the interference pressure field requires the solution of an integral equation. Since the solution was not found, it was necessary to resort to a tedious numerical summation process.

SYMBOLS

c	wing chord
C_1, C_2, C_3	factors for determining wing pressure coefficients
c_d	section drag coefficient
d	body diameter

k_1, k_2, k_3	factors for determining average normal velocity at control area due to set of rectangular wedges
m	cotangent of sweep angle of line pressure source
M_o	free-stream Mach number
n_1, n_2, n_3, n_4	averages used in determining section drag coefficient
p	local static pressure
p_o	free-stream static pressure
P	pressure coefficient $\left(\frac{p-p_o}{q_o}\right)$
q_o	free-stream dynamic pressure
r.p.	real part of a complex function
s	semispan of wing measured from wing-body juncture to wing tip
s_o	semispan of rectangular wedge
t	maximum thickness of double-wedge section
u,v,w	perturbation velocities of line pressure source
u_w, v_w, w_w	perturbation velocities for rectangular wedge in x_w, y_w, z_w directions, respectively
v_n	finite velocity normal to body (positive outward) due to leading-edge sources after reduction of infinite sidewash velocities to finite velocities
$\bar{v}_n$	average finite normal velocity for control area
$\bar{v}_n'$	average velocity normal to control area due to rectangular wedge
V_o	free-stream velocity

x,y,z — longitudinal, lateral, and normal coordinates for line pressure source or sink with source or sink in $z=0$ plane and the origin of the source or sink at $x=0$, $y=0$ (The positive x direction is downstream, the positive y direction is from the x axis toward the source or sink, and the positive z direction is upward.)

x',y',z' — oblique coordinates ($x'=x-my$, $y'=y-mx$, $z'=z\sqrt{1-m^2}$)

x_w, y_w, z_w — longitudinal, lateral, and normal coordinates for rectangular wedge with chord plane of wedge coinciding with $z_w=0$ plane (The positive x_w direction is downstream, the the positive y_w direction to the right for an observer looking upstream, and the positive z_w direction away from the body.)

$\left(\frac{dz}{dx}\right)_s$ — slope of streamwise section due to line pressure source or sink (Positive for a source and negative for a sink.)

$\left(\frac{dz}{dx}\right)_A, \left(\frac{dz}{dx}\right)_B, \left(\frac{dz}{dx}\right)_C$ — streamwise slope of rectangular wedges corresponding to strips A, B, and C, respectively

$\left(\frac{dz}{dx}\right)_{A-I}$ — streamwise slope of rectangular wedge corresponding to strip A and the region of influence which starts at the forward edge of control area A–I

$\left(\frac{dz}{dx}\right)_w$ — slope of rectangular wedge in streamwise direction

$\left(\frac{\bar{v}_n}{V_o}\right)_A, \left(\frac{\bar{v}_n}{V_o}\right)_B, \left(\frac{\bar{v}_n}{V_o}\right)_C$ — ratio of average finite normal velocity to free-stream velocity for control areas of strips A, B, and C, respectively

$\Delta\left(\frac{\bar{v}_n}{V_o}\right)$ — change in ratio of the average finite normal velocity to the free-stream velocity due to a given ring of rectangular wedges

$\left(\frac{\bar{v}_n}{V_o}\right)_{A-I}$ ratio of average finite normal velocity to free-stream velocity for control area A-I

φ potential of the perturbation velocities of a line pressure source or sink

θ polar angle in planes perpendicular to body with origin at intersection of plane with body axis (The $\theta=0$ plane corresponds to the right half-wing for an observer facing the oncoming stream and θ is positive counterclockwise.)

ξ, η, ζ longitudinal, lateral, and normal coordinates with the origin at the leading edge of the wing-body juncture and the $\zeta=0$ plane coincident with the chord plane of the wing (The positive ξ direction is downstream, and the positive ζ direction is up. The positive η direction is taken to the right of an observer facing the oncoming stream for the right half-wing and is taken to the left for the left half-wing.)

ANALYSIS

Components of the Interference Pressure Drag

The interference pressure drag for a wing-body combination is the difference between the drag of the wing-body combination and the sum of the drags of the body alone and the wing alone. The wing alone is used in this report to mean the two exposed half-wings joined together. The interference pressure drag arises from the following pressure distributions: (1) The pressure distribution on the body in combination minus that on the body alone, and (2) the pressure distribution on the wing in combination minus that on the wing alone. This report considers a symmetrical wing mounted on the cylindrical portion of a pointed body of revolution. The longitudinal axes of the body and wing are in the stream direction. Since the sides of the body in the region influenced by the wing are then parallel to the flow, the body has no interference pressure drag. Thus, the interference pressure drag is the difference in the drags of the wing in combination and of the wing alone. The methods of references 5 or 6 can be used to determine the drag of the wing alone, but no method has hitherto existed for determining the pressure distribution and drag

of the wing in combination. It is the purpose of this report to present such a method.

Components of Pressure Field on Half-Wing in Combination

In the following analysis of the pressure distribution and drag of either half-wing in combination, the pressure field acting on the half-wing is subdivided into four components: (1) That due to the part of the body forward of the region of influence of the wing, (2) that due to the given half-wing, (3) that due to the opposite half-wing, and (4) that due to interaction between the half-wings and the part of the body within their region of influence. This subdivision of the pressure field acting on the half-wing in combination is convenient for the purposes of the analysis. However, once the method of the analysis has been established, a slightly different point of view will be adopted.

Consider now methods for determining the various components. The first component can be determined by any of the methods available for determining the pressure field of bodies of revolution, such as the method of characteristics or the method of reference 7. In general, this component is different for each body shape and no further account will be taken of it in the analysis. The second and third components can be determined by the method of reference 5. This method is considered briefly in this report since it is the starting point of the analysis to obtain the fourth component, which is the one to which the analysis is principally devoted. It should be noted that the part of the body forward of the region of influence of the wings will cause only small perturbation velocities at the wing and will have only a second-order effect on the fourth component of the pressure field.

Pressure Field on Half-Wing Due to Itself and Opposite Half-Wing

The line pressure source solution of the linearized equation of supersonic flow is fundamental in determining the pressure field on either half-wing due to itself or to the opposite half-wing. Jones (reference 5) gives for the streamwise perturbation velocity u of a line pressure source swept behind the Mach cone

$$u = \text{r.p.} - \frac{V_Q}{\pi} \frac{m}{\sqrt{1-m^2}} \left(\frac{dz}{dx}\right)_s \cosh^{-1} \frac{x'}{\sqrt{y'^2+z'^2}}$$

The velocity potential for the line pressure source is obtained by integration of the foregoing equation along a path parallel to the x axis. This gives

$$\varphi = \int_{-\infty}^{x} u\,dx = \frac{V_o}{\pi\sqrt{1-m^2}} \left(\frac{dz}{dx}\right)_s \left\{ y' \cosh^{-1}\left(\frac{x'}{\sqrt{y'^2+z'^2}}\right) - y\sqrt{1-m^2}\cosh^{-1}\left(\frac{x}{\sqrt{y^2+z^2}}\right) + z' \cos^{-1}\left[\frac{yy'+z^2}{\sqrt{(y^2+z^2)(y'^2+z'^2)}}\right]\right\} \tag{2}$$

The lateral and vertical perturbation velocity components are obtained by differentiating equation (2) as follows:

$$v = \frac{\partial\varphi}{\partial y} = \frac{V_o}{\pi}\left(\frac{dz}{dx}\right)_s \left[\frac{1}{\sqrt{1-m^2}}\cosh^{-1}\left(\frac{x'}{\sqrt{y'^2+z'^2}}\right) - \cosh^{-1}\left(\frac{x}{\sqrt{y^2+z^2}}\right)\right] \tag{3}$$

$$w = \frac{\partial\varphi}{\partial z} = \frac{V_o}{\pi}\left(\frac{dz}{dx}\right)_s \cos^{-1}\left[\frac{yy'+z^2}{\sqrt{(y^2+z^2)(y'^2+z'^2)}}\right] \tag{4}$$

To illustrate the nature of the downwash and sidewash, these fields have been calculated from equations (3) and (4) for a sweepback angle of 60° and a free-stream Mach number of $\sqrt{2}$. The results of the calculations are presented in figures 1 and 2. These figures show the downwash and sidewash patterns in any plane perpendicular to the axis of the Mach cone of the source. Since the flow is conical, the downwash and sidewash velocities depend only on y/x and z/x, the ratios which determine the direction of any ray from the apex of the Mach cone. The line source starts at the apex of the Mach cone and pierces any plane perpendicular to the axis of the Mach cone at a point $y/x=0.577$ and $z/x=0$. Figure 1 reveals that upwash exists above the plane of the source, and downwash exists beneath it. Between the line source and the axis of the Mach cone, the upwash and downwash velocities are constant just above and below the zero plane and their magnitudes are equal. Thus, behind the line source there exists, in effect, a symmetrical wing with a wedge-shaped streamwise section.

(In the linearized theory of supersonic flow, the surfaces of the wing are displaced only infinitesimally from the $z=0$ plane.) In the rest of the $z=0$ plane, the downwash velocity is zero. The sidewash pattern of figure 2 is symmetrical above and below the $z=0$ plane. There is positive infinite sidewash velocity along the line pressure source and negative infinite sidewash velocity along the axis of the Mach cone.

The fact that a line pressure source or sink produces zero downwash velocity everywhere in the zero plane except directly behind it simplifies the simulation of complicated wings by the superposition of line sources and sinks. In fact, the pressure field of any wing which is symmetrical above and below the $z=0$ plane and the surfaces of which are composed of planes can easily be simulated by a finite number of line sources and sinks. For instance, the pressure field of an untapered, swept-back half-wing of symmetrical double-wedge section with the maximum thickness at the midchord would be formed by the source-sink system shown in figure 3. The leading-edge and trailing-edge sources are of equal strength, but the midchord-line sink is twice as strong as each of the sources. A source and two sinks are introduced to form a tip. In determining the pressure field of the half-wing from its source-sink system, the u perturbation velocity for each source or sink is determined from equation (1) for a given point on the wing, taking into account the fact that the starting point of each source or sink is taken as the origin of the x,y,z coordinate system in determining its particular value of u. The pressure coefficients of the line sources and sinks are then determined from the following equation which is based on linear theory:

$$P = -2\left(\frac{u}{V_o}\right) \tag{5}$$

Finally, the pressure coefficients are summed to give the pressure coefficient of the half-wing at the particular point.

In determining the drag of the half-wing from the pressure field, it is not necessary to consider the contributions of the tip source-sink system to the wing pressures when the Mach lines of the tip source and sinks on a given half-wing intersect the trailing edge of this half-wing. In this instance, which is frequently the case, the tip source-sink system changes only the distribution of drag within its region of influence but does not change the over-all drag. (See references 8 and 9.)

The determination of the pressure field on one half-wing due to

the other half-wing is simplified by the fact that one half-wing does not produce any downwash in the plane of the other half-wing (fig. 1). Hence, the pressure field due to the one can be considered to act directly on the other. Figure 4 presents an example of the interaction of the pressure fields of two half-wings separated by half a chord length. For the configuration shown, the leading- and trailing-edge sources, as well as the midchord sinks, all contribute to the pressures on the opposite half-wing. In computing the contributions, it should be noted that the value of y to be used in determining y' in equation (1) will be negative. In this particular case, the tip system of one half-wing does not contribute to the pressures on the opposite half-wing.

Pressure Field on Half-Wing Due to Interaction Between Half-Wings and Body

The source-sink system which represents the half-wings will induce both downwash and sidewash against that portion of the body within their region of influence. However, the velocity normal to the body must be zero everywhere. This constraining action of the body affects the wing pressures and gives rise to the fourth component of the pressure field acting on the half-wings in combination. To determine this component of the pressure field, it is necessary to find solutions of the linearized equation for supersonic flow which will cancel the normal velocity induced at the body surface by the half-wings and which will have no contribution to the downwash in the plane of the wing. It is apparent that a method for determining that part of the fourth component associated with the leading-edge sources will be equally applicable to determining those parts due to the midchord-line sinks and the trailing-edge sources. For certain restricted conditions, such as for wings of very low aspect ratio or for very low supersonic Mach numbers, the tip source-sink systems may have an effect on the fourth component of the pressure distribution on the half-wing. However, the possible effect of the tip systems is ignored in the rest of the analysis, and only the leading-edge sources are considered.

Reference to figures 1 and 2 shows that infinite normal velocity can arise from the sidewash only. Infinite sidewash velocity is induced against the body along the intersections of the body with the wing-chord plane. Finite downwash and sidewash velocities are induced everywhere else on the body. It is convenient to reduce the infinities in the normal velocity field to finite values and then to cancel the finite residue. As will be shown next, this infinite sidewash can be reduced by a source-sink system.

Reduction of infinite values of sidewash velocity to finite values by source–sink system.– The infinite sidewash velocities normal to the body in the $\zeta=0$ plane due to the leading-edge sources can be reduced to finite velocities by means of the source–sink system shown in figure 5. Image source II cancels identically the infinite sidewash velocities due to source I, and image source V cancels identically those due to source IV. The image sources, however, produce infinite sidewash velocities along themselves (fig. 2) and produce downwash velocities behind themselves which interfere with the wing boundary conditions. These two conditions require the addition of image sinks III and VI, the origins of which lie on the image sources inside the body. As shown in figure 5, the origins of the image sinks are displaced from the origins of the corresponding sources. (Otherwise the sinks would identically cancel the sources.) It is noteworthy that the infinite sidewash velocities along the image sources are not identically canceled by the infinite sidewash velocities of the corresponding image sinks because of the displacement of their origins. The resultant sidewash velocity at the body is, however, finite. To accomplish the reduction of the infinities in a satisfactory manner, the origins of the image sinks must be close to the origins of the corresponding image sources. This point will be considered in detail in the subsequent illustrative example.

The contribution to the pressure distribution of the wing due to reduction of the infinite sidewash is readily obtained. It is the sum of the pressure coefficients due to the sources II and V, and sinks III and VI as determined from equations (1) and (5). Again, the origin of the x,y,z coordinate system is taken at the starting point of the particular source or sink for which the calculation of the pressure coefficient is being made.

After the infinite sidewash velocities have all been reduced to finite values, there remains a distribution of finite velocity normal to the surface of the body. The part of the fourth component of the wing pressure field arising from canceling these finite normal velocities will be only approximately determined.

Approximate cancellation of the finite normal velocities by rectangular wedges.– The finite velocity normal to the body at any point after the cancellation of the infinite sidewash may be determined with the aid of equations (3) and (4). From these equations the sidewash and downwash due to sources I, II, IV, and V and sinks III and VI are determined, and are then summed by the following equation to obtain the finite velocity normal to the body:

$$\frac{v_n}{V_o} = \sum_{i=I}^{i=VI} \left(\frac{v}{V_o}\right)_i \cos\theta + \sum_{i=I}^{i=VI} \left(\frac{w}{V_o}\right)_i \sin\theta \qquad (6)$$

The right-hand sideline of the body for an observer facing upstream corresponds to $\theta=0^\circ$, and the left-hand sideline to $\theta=180^\circ$. A positive v_n/V_o denotes flow out of the body with v positive to the right (looking forward) and w positive upward. Only the normal velocity distribution for values of θ from 0° to 90° need be considered since the flow is similar in every quadrant of the body.

The surface of the circular cylindrical body is now divided into control areas, the number of which determines the accuracy of the solution. These control areas are formed by the intersections of longitudinal strips with a number of rings as shown in figure 6. Eight longitudinal strips and eighteen rings were selected in the present analysis to provide a reasonable compromise between accuracy and work required. Strip A (fig. 6) has a perpendicular tangent to the plane of the wing, and the value of θ for this strip varies from -22.5° to $+22.5^\circ$. The rings are 0.2d wide and start at $\xi=0$, where the leading-edge sources intersect the body.

The next step in the analysis is to present a method for canceling the average flow induced through each control area by leading-edge sources. The finite normal velocities at every point on the body surface can, in principle, be identically canceled by a distribution on the surface of point sources of the type used by Puckett in reference 6. For a plane distribution of these sources, the local source strength is proportional to the local induced vertical velocity. However, when the sources are placed on a curved surface, this simple relationship no longer holds, and the determination of the surface distribution of the source strength to cancel an arbitrary surface distribution of normal velocity involves the solution of an integral equation. Since the solution of this equation was not obtained, it was necessary to use an approximate method.

The approximate method used to cancel the average finite normal velocity at each control area employs the solution for a rectangular wedge of infinite chord. The rectangular wedge is formed by the source-sink system shown in figure 7. The sources and sinks all have no sweep and correspond to $m=\infty$. For $m=\infty$, the u, v, and w velocity components of a source given by equations (1), (3), and (4) reduce to

$$u = -\frac{V_o}{\pi}\left(\frac{dz}{dx}\right)_s \cos^{-1}\left(\frac{-y}{\sqrt{x^2-z^2}}\right) \tag{7}$$

$$v = -\frac{V_o}{\pi}\left(\frac{dz}{dx}\right)_s \cosh^{-1}\left(\frac{x}{\sqrt{y^2+z^2}}\right) \tag{8}$$

$$w = \frac{V_o}{\pi}\left(\frac{dz}{dx}\right)_s \cos^{-1}\left(\frac{-xy}{\sqrt{x^2-z^2}\sqrt{y^2+z^2}}\right) \tag{9}$$

The u, v, and w components for the rectangular wedge with the origin as shown in figure 7 are

$$u_w = -\frac{V_o}{\pi}\left(\frac{dz}{dx}\right)_w \left\{\pi - \cos^{-1}\left[\frac{-(y_w-s_o)}{\sqrt{x_w^2-z_w^2}}\right] - \cos^{-1}\left(\frac{y_w+s_o}{\sqrt{x_w^2-z_w^2}}\right)\right\} \tag{10}$$

$$v_w = \frac{V_o}{\pi}\left(\frac{dz}{dx}\right)_w \left\{\cosh^{-1}\left[\frac{x_w}{\sqrt{(y_w-s_o)^2+z_w^2}}\right] - \cosh^{-1}\left[\frac{x_w}{\sqrt{(y_w+s_o)^2+z_w^2}}\right]\right\} \tag{11}$$

$$w_w = \frac{V_o}{\pi}\left(\frac{dz}{dx}\right)_w \left\{\pi - \cos^{-1}\left[\frac{-x_w(y_w-s_o)}{\sqrt{x_w^2-z_w^2}\sqrt{(y_w-s_o)^2+z_w^2}}\right] - \cos^{-1}\left[\frac{x_w(y_w+s_o)}{\sqrt{x_w^2-z_w^2}\sqrt{(y_w+s_o)^2+z_w^2}}\right]\right\} \tag{12}$$

The rectangular wedges are placed on the sides of a regular octagonal prism inside the body as shown by figure 8. From symmetry considerations, it is apparent that the wedge angles, or slopes, of the rectangular wedges to be used are identical for the two vertical sides of the prism, the two horizontal sides, and the four inclined sides. It is also apparent that no flow will be induced across the plane of the wing, and therefore the wing boundary conditions are satisfied. The rectangular wedges would induce infinite normal velocities at the cylindrical surface if the octagonal prism were inscribed in the circular body. To avoid this difficulty, the octagonal prism has arbitrarily been inscribed inside a cylinder

concentric with the body and having a diameter 0.96d. Rectangular wedges are quite suitable for the present purpose since it is necessary only to satisfy the boundary conditions at the body surface and not at positions inside the body.

A step-by-step process is used in determining the slopes of the rectangular wedges. First, rectangular wedges are placed on the octagonal prism so that their region of influence on the body begins at the $\xi=0$ plane (fig. 6). From equations (11) and (12) for the downwash and sidewash, the ratio of average normal velocity to free-stream velocity $\bar{v}_n'/V_o$ through any control area due to the rectangular wedge on side A of the octagonal prism is then determined. This average normal velocity ratio is dependent on a factor k which is different for each control area as follows:

$$\frac{\bar{v}_n'}{V_o} = k\left(\frac{dz}{dx}\right)_A \tag{13}$$

where $(dz/dx)_A$ refers to the slope of the rectangular wedge corresponding to strip A. The values of k for all control areas above the horizontal plane of symmetry have been determined. The value of the normal velocity was calculated with the help of equations (11) and (12) for a number of points on the body and $\bar{v}_n'/V_o$ for each control area was determined by a process of cross-plotting and integrating with a planimeter. Finally, the values of k were determined so that equation (13) was fulfilled. Table I gives the factor k for the various control areas due to the rectangular wedge on side A of the octagonal prism. The table presents results for only half the body since the results are similar above and below the plane of the wing. It is apparent that the factors in table I may be used to determine the average normal velocity through any control area due to any rectangular wedge.

With the aid of the factors in table I, the slopes of the rectangular wedges required to cancel the average finite normal velocity ratio $\bar{v}_n/V_o$ in every control area of ring I can be determined. Let $(dz/dx)_{A-I}$ be the slope of the wedges which lie on sides A and E of the prism (fig. 8) and the regions of influence of which start on the body at $\xi=0$ (fig. 6). Let $(dz/dx)_{B-I}$ be the corresponding slope of the wedges for sides B, D, F, and H and $(dz/dx)_{C-I}$ the slope of the wedges for sides C and G. Now let $(\bar{v}_n/V_o)_{A-I}$ be the ratio of the average finite normal velocity to the free-stream velocity for control areas A-I and E-I, $(\bar{v}_n/V_o)_{B-I}$ that for control

areas B–I, D–I, F–I, and H–I, and $(\bar{v}_n/V_o)_{C-I}$ that for control areas C–I and G–I. Consider now control area A–I. On the basis of the factors in table I, the ratio of average normal velocity to free-stream velocity induced through this control area by the wedge of side A corresponds to $0.813(dz/dx)_A$. Since a wedge of given slope on side A will induce the same normal velocities through control area B–I as a wedge of identical slope on side B will induce through control area A–I, it follows from table I that the ratio of average normal velocity to free-stream velocity induced through control area A–I by the wedge on side B is $0.069(dz/dx)_{B-I}$. By symmetry, the wedge on side H will also have the contribution $0.069(dz/dx)_{B-I}$. The wedges on sides C, D, E, F, and G have no contribution because the control area A–I is outside their regions of influence for the Mach number and size of control area selected in the analysis. Since the average velocity normal to control area A–I is to be zero

$$\left(\frac{\bar{v}_n}{V_o}\right)_{A-I} + 0.813\left(\frac{dz}{dx}\right)_{A-I} + 2(0.069)\left(\frac{dz}{dx}\right)_{B-I} = 0 \qquad (14)$$

Similarly, for control areas B–I and C–I, there is obtained

$$\left(\frac{\bar{v}_n}{V_o}\right)_{B-I} + 0.813\left(\frac{dz}{dx}\right)_{B-I} + 0.069\left[\left(\frac{dz}{dx}\right)_{A-I} + \left(\frac{dz}{dx}\right)_{C-I}\right] = 0 \qquad (15)$$

and

$$\left(\frac{\bar{v}_n}{V_o}\right)_{C-I} + 0.813\left(\frac{dz}{dx}\right)_{C-I} + 2(0.069)\left(\frac{dz}{dx}\right)_{B-I} = 0 \qquad (16)$$

The simultaneous solution of equations (14) to (16) gives the slopes of the rectangular wedges,

$$\left(\frac{dz}{dx}\right)_{A-I} = -1.248\left(\frac{\bar{v}_n}{V_o}\right)_{A-I} + 0.2151\left(\frac{\bar{v}_n}{V_o}\right)_{B-I} - 0.01825\left(\frac{\bar{v}_n}{V_o}\right)_{C-I} \qquad (17)$$

$$\left(\frac{dz}{dx}\right)_{B-I} = 0.1075\left[\left(\frac{\bar{v}_n}{V_o}\right)_{A-I} + \left(\frac{\bar{v}_n}{V_o}\right)_{C-I}\right] - 1.267\left(\frac{\bar{v}_n}{V_o}\right)_{B-I} \qquad (18)$$

$$\left(\frac{dz}{dx}\right)_{C-I} = -0.01825\left(\frac{\overline{v}_n}{V_o}\right)_{A-I} + 0.2151\left(\frac{\overline{v}_n}{V_o}\right)_{B-I} - 1.248\left(\frac{\overline{v}_n}{V_o}\right)_{C-I} \quad (19)$$

These values of $(dz/dx)_{A-I}$, $(dz/dx)_{B-I}$, and $(dz/dx)_{C-I}$ are such that the average normal velocity for each control area of ring I is zero.

Once the slope of the rectangular wedges required to cancel the average finite normal velocities in the control areas of ring I are determined from equations (17) to (19), the values of $\overline{v}_n/V_o$ for all the control areas behind ring I must be adjusted for the contributions due to these rectangular wedges. The adjustment need be made only for strips A, B, and C because of symmetry. Consider, for example, control area B-VII. Due to the wedge on side A of the octagonal prism, the ratio of average normal velocity to free-stream velocity for this control area is $0.218(dz/dx)_{A-I}$, using the factors of table I. Consider now the contribution of the wedge on side E. From symmetry, the effect on control area B-VII of the wedge on side E is the same as the effect on control area D-VII of the wedge on side A. Thus the contribution of the wedge on side E to the ratio of average normal velocity to free-stream velocity for control area B-VII is $0.165(dz/dx)_{A-I}$. The total contribution of sides A and E is thus $(0.218 + 0.165)\ (dz/dx)_{A-I}$. In a similar manner, using the factors of table I, it can be shown that the total contribution for the wedges of sides B, D, F, and H is $(0.835 + 0.153 + 0.180 + 0.153)\ (dz/dx)_{B-I}$ and that the sum contribution of sides C and G is $(0.218 + 0.165)\ (dz/dx)_{C-I}$. From this example, it can be seen that the contribution to the ratio of average normal velocity to free-stream velocity due to the rectangular wedges of a given ring can be represented as

$$\Delta\left(\frac{\overline{v}_n}{V_o}\right) = k_1\left(\frac{dz}{dx}\right)_A + k_2\left(\frac{dz}{dx}\right)_B + k_3\left(\frac{dz}{dx}\right)_C \quad (20)$$

The values of k_1, k_2, and k_3 have been determined in the foregoing manner for all the control areas of strips A, B, and C. The factors k_1, k_2, and k_3, due to the rectangular wedges of ring I, are presented in table II. When these factors are used, the values of $\overline{v}_n/V_o$ for the control areas behind ring I are readily adjusted for the normal velocity induced by the rectangular wedges of ring I.

The foregoing process is repeated in the step-by-step solution. A second set of rectangular wedges is placed on the octagonal prism

so that the region of influence on the body begins at the boundary between rings I and II at $\xi=0.2d$. The average finite normal velocities for the control areas of ring II are then canceled in the same manner as for ring I, using equations (17), (18), and (19), but substituting the quantities $(\overline{v}_n/V_o)_{A-II}$, $(\overline{v}_n/V_o)_{B-II}$, and $(\overline{v}_n/V_o)_{C-II}$ for $(\overline{v}_n/V_o)_{A-I}$ $(\overline{v}_n/V_o)_{B-I}$, and $(\overline{v}_n/V_o)_{C-I}$, respectively, and solving for the quantities $(dz/dx)_{A-II}$, $(dz/dx)_{B-II}$, and $(dz/dx)_{C-II}$. The values of $\overline{v}_n/V_o$ for all control areas behind ring II are adjusted as previously, using equation (20) and the factors of table II. In using the factors of table II, however, it must be borne in mind that ring II is farther downstream than ring I. Thus, for instance, the average normal velocity induced at control B-VII by the wedges of ring II would be the same as that induced at control area B-VI by the wedges of ring I. Thus, for the control area B-VII, using the factors in table II,

$$\Delta\left(\frac{\overline{v}_n}{V_o}\right)_{B-VII} = 0.433\left(\frac{dz}{dx}\right)_{A-II} + 1.412\left(\frac{dz}{dx}\right)_{B-II} + 0.433\left(\frac{dz}{dx}\right)_{C-II} \tag{21}$$

In the foregoing manner, the slopes of the wedges for ring II are determined, and the average normal velocities for all control areas behind ring II are adjusted for the normal velocities induced by the wedges of ring II.

The procedure used in determining the slopes of the wedges for ring I and adjusting the control areas behind ring I for the induced normal velocities of the wedges of ring I has been applied to ring II. It is clear that this procedure must also be applied to each additional ring in the order III, IV, V, etc., through the last ring, that is, through the last ring the region of influence of which intersects the wing. With regard to the procedure, it is desirable to emphasize the use of table II. Consider the contribution to the ratio $(\overline{v}_n/V_o)$ at control area B-VII due to the wedges of ring VI. This contribution will be the same as that at control area B-II due to the rectangular wedges of ring I. Thus, for the effect of ring VI on control area B-VII

$$\Delta\left(\frac{\overline{v}_n}{V_o}\right)_{B-VII} = 0.189\left(\frac{dz}{dx}\right)_{A-VI} + 0.887\left(\frac{dz}{dx}\right)_{B-VI} + 0.189\left(\frac{dz}{dx}\right)_{C-VI} \tag{22}$$

The procedure to determine the slopes of the rectangular wedges is now summarized. Equations (17), (18), and (19) are solved to obtain the slopes of the wedges for ring I. The values of $(\overline{v}_n/V_o)$ for all control areas behind ring I are adjusted for the normal velocity induced by the wedges of ring I using equation (20) and the factors of table II. The slopes of the rectangles of ring II are then determined using equations similar to equations (17), (18), and (19) with identical coefficients. The values of $\overline{v}_n/V_o$ for all control areas behind ring II are adjusted using equation (20) and the factors of table II, and the process is repeated through the last ring that can influence the wing pressures.

From the slopes of the wedges, that part of the fourth component of the pressure field acting on the half-wing in combination which is due to canceling the average finite normal velocity at each control area can be calculated. This calculation completes the determination of the pressure field acting on the half-wing in combination. The pressure coefficient at any point due to any one of the rectangular wedges can be calculated with the help of equations (5) and (10). It can be easily shown that the pressure coefficient at any point on the wing due to the first set of rectangular wedges can be expressed in the form

$$P = C_1\left(\frac{dz}{dx}\right)_{A-I} + C_2\left(\frac{dz}{dx}\right)_{B-I} + C_3\left(\frac{dz}{dx}\right)_{C-I} \qquad (23)$$

The contributions of the other sets of rectangular wedges to the pressure at a given point can be similarly expressed and calculated. The contributions of all of the sets are summed at a number of points at a given spanwise station to yield the section pressure distribution. The details of calculating the pressure coefficients will be given in the example.

ILLUSTRATIVE EXAMPLE

The pressure field acting on a half-wing in combination has been subdivided into four components in a particular manner to facilitate the analysis. The fourth component, that due to interaction between half-wings and body, was further subdivided into two parts. With the determination of its various components, the pressure distribution on a half-wing is fully determined. The part of this pressure distribution due to interference will be considered in this illustrative

example. The over-all interference pressure distribution of the half-wing in combination is defined for the purpose of this report to be the sum of that component due to the opposite half-wing and that component due to interaction between the half-wings and body. The component due to the body nose is not considered for reasons already given, and the component due to the effect of the half-wing on itself is not an interference pressure distribution. The over-all interference pressure distribution is considered in two parts to facilitate the fairing of curves required in this illustrative example. The first part of the over-all interference pressure distribution is the sum of the pressure distribution due to the opposite half-wing and the pressure distribution due to reducing the infinite sidewash velocities to finite velocities. The second part is the pressure distribution due to canceling the average normal velocities at each control area by rectangular wedges.

In this illustrative example the interference pressure distribution at zero lift and the interference pressure drag are calculated at $M_o = \sqrt{2}$ for a 60° swept-back wing mounted on a circular cylindrical body. The dimensions of the wing-body configuration considered are given in figure 9. An untapered swept-back wing has been chosen which has a symmetrical double-wedge section with the maximum thickness at the midchord, and the body diameter has been taken equal to one-half the wing chord. The over-all interference pressure distributions due to the leading-edge sources have been determined for the stations shown in figure 9. The spanwise distribution of pressure drag corresponding to the over-all interference pressure distributions has been calculated. Finally, the interference pressure drag, as defined in the analysis, has been determined.

Wing Pressure Field Due to Leading-Edge Source of Opposite Half-Wing and to Canceling Infinite Sidewash of Leading-Edge Sources

The pressure distribution at the wing-body juncture of the right half-wing (for an observer looking forward) due to the leading-edge source of the left half-wing and due to reducing the infinite sidewash velocities of the leading-edge sources to finite velocities is shown in figure 10. Only the interference pressure distribution due to the leading-edge sources is shown for purposes of clarity. The corresponding pressure distribution for the midchord-line sinks is double that for the leading-edge sources, is negative, and is shifted a half of a chord rearward. The corresponding pressure distribution for the trailing-edge sources is identical to that for the leading-edge sources but is shifted a chord length rearward.

In figure 10 the contribution of the leading-edge source of the left half-wing is that due to source IV and the contribution due to reducing the infinite sidewash velocities of the leading-edge sources is represented by the sum of sources II and V plus sinks III and VI. The total effect is II + III + IV + V + VI as shown.

These pressure distributions present several noteworthy features: First, the wing pressures due to reducing the infinite sidewash velocities are all finite since the infinite pressure peak of source V is canceled, although not identically, by the infinite pressure peak of sink VI without forming a cusp. A cusp near the leading edge arises in the sum pressure distribution (II + III + IV + V + VI) due to sink III. The position of this cusp depends only on the position of the origin of sink III, which is arbitrary. As the origin of sink III approaches that of source II, it is apparent that the effect of the cusp is made smaller. Two cusps are introduced into the sum pressure distribution at the intersections of the Mach lines of source V and sink VI with the wing-body juncture. As the origin of sink VI approaches the origin of source V, the difference in the heights of the cusps decreases as well as the chordwise distance between them. For reasons that will subsequently be discussed, it is desirable to minimize the effect of the cusps in the final pressure distribution by locating the origins of sinks III and VI close to the origins of sources II and V, respectively. It was found that positions of the origins of sinks III and VI of either 0.05d or 0.10d from the wing-body juncture gave good results in the present example, as will be pointed out. If the origins of the sinks are located too close to the origins of their respective sources, however, the finite velocities normal to the body (v_n) would be too large along the wing-body junctures and would impair the accuracy of the method.

The pressure distribution in figure 10 represents only part of the interference pressure distribution at the wing-body juncture due to the leading-edge sources. The second part arises from canceling the finite velocities normal to the body. As previously mentioned, a distribution of point sources of the type used by Puckett scattered over the body could, in principle, cancel the values of v_n/V_o at every point on the body. The pressure distribution at the wing-body juncture resulting from this source distribution would have cusps that would directly offset those of figure 10. However, in the present approximate method of obtaining the second part of the interference pressure field, the offsetting cusps will not be obtained.

The manner in which the pressure distribution, due to the leading-edge source of the opposite half-wing and to reduction of the infinite sidewash velocities of the leading-edge sources, varies in the spanwise

direction is shown in figure 11. Near the leading edge of the wing-body juncture ($\eta/s=0$) the pressure coefficient is large. This is to be expected, as will be pointed out. The pressure coefficients are all zero at the forward Mach line for all stations except the wing-body juncture, and the first cusp reduces in severity as the spanwise distance increases. Although the double cusp near the midchord of the inboard station reduces in severity as the spanwise distance increases, it does not do so as rapidly as the cusp behind the leading-edge Mach line. The parts of the pressure distributions between the leading edge and the leading-edge Mach line have been included in the figure because these distributions are moved downstream in determining the corresponding contributions of the midchord-line sinks and the trailing-edge sources on the wing.

Wing Pressure Field Due to Approximate Cancellation of the Finite Velocities Normal to the Body Due to Leading-Edge Sources

The part of the interference pressure field due to approximate cancellation of the finite velocities normal to the body has been determined only for the leading-edge sources as before. First, the ratio of the average finite normal velocity to free-stream velocity $\bar{v}_n/V_o$ for each control area after cancellation of the infinite sidewash was determined. The values of v/V_o and w/V_o for sources I, II, IV, and V and sinks III and VI (fig. 5) were calculated for values of θ of 0°, 10°, 30°, 60°, and 90°, and for distances ξ/d of 0, 0.5, 1.0, 1.5, 2.0, 2.5, and 3.0, using equations (3) and (4). The values of v_n/V_o were then calculated from equation (6). The values of v_n/V_o were plotted against ξ/d for each value of θ and averaged over the intervals 0 – 0.2, 0.2 – 0.4, etc. These average quantities were then plotted against θ and averaged over the intervals 0 – 22.5°, 22.5° – 67.5°, and 67.5° – 90° for each control ring giving $\bar{v}_n/V_o$ for each control area. The values of $\bar{v}_n/V_o$ for the control areas are given in table III.

The next step was to determine the slopes of the rectangular wedges necessary to cancel the ratio of average finite normal velocity to free-stream velocity $\bar{v}_n/V_o$ for each control area. The slopes $(dz/dx)_{A-I}$, $(dz/dx)_{B-I}$, and $(dz/dx)_{C-I}$ for ring I were calculated from equations (17), (18), and (19). The values of $\bar{v}_n/V_o$ for the control areas of rings II to XVIII were adjusted using equation (20) and the factors in table II. Next, the values of $(dz/dx)_{A-II}$, $(dz/dx)_{B-II}$, and $(dz/dx)_{C-II}$ for ring II were determined, and the process was continued to ring XVIII, the last ring affecting the wing pressures. The slopes of the rectangular wedges are given in table IV.

The chordwise pressure distributions due to the approximate cancellation of the finite velocities normal to the body were finally determined using equation (23). Some consideration was given to choosing the chordwise positions at which the pressure coefficients of the wing–body juncture were to be calculated. Consider sides A and E of the octagonal prism in figure 8. The rectangular wedges on these sides will have leading-edge shock waves which intersect the wing surface. For a short distance behind the shock waves a constant pressure exists. Calculation shows that the constant pressure region covers 6 percent of the chord at the wing–body juncture but only 0.5 percent at the $\eta/s=1.0$ station because of the effect of the tip Mach cones of the wedge. At the end of the constant pressure region the chordwise pressure distribution has a vertical tangent, and the pressure coefficient falls rapidly to a much lower value a short distance back. The points at which the pressure coefficients were calculated were chosen so that they did not coincide with the constant pressure peaks at the wing–body juncture. The distance between the points was taken equal to the width of the rings (0.1c or 0.2d for the present example) to simplify the calculations.

The coefficients C_1, C_2, and C_3 used in equation (23) in calculating the contributions to the chordwise pressure distributions of the first set of rectangular wedges are presented in table V. The contributions of the second set of rectangular wedges to the wing pressure coefficients were also calculated using equation (23) and table V, taking account of the fact that the second set of wedges start a distance 0.2d downstream of the first set. The factors for the first set of wedges are $C_1=0.4462$, $C_2=0.8613$, and $C_3=0.4168$ at the 0.582 chord position of the 0.05 η/s station; whereas the factors for the second set of rectangular wedges are $C_1=0.6858$, $C_2=1.2024$, and $C_3=0.5396$ at this point. Thus, the contribution of all rectangular wedges to the pressure coefficient at any point was readily summed.

The pressure distributions due to canceling approximately the finite velocities normal to the body due to the leading-edge sources are shown in figure 12 for four of the seven spanwise stations. Since the outer stations are farthest from the wedges, the scatter of the points decreases and the accuracy improves as the distance from the body increases. Curves have been faired through the points of the 18-ring solution. For purposes of comparison, the points of the chordwise pressure distribution using a 9-ring solution with the width of the rings equal to 0.4d have also been plotted. These points scatter about the curves for the 18-ring solution, but the scatter is not much greater than that of the more accurate method. Apparently, the degree of approximation does not change rapidly with the number of rings chosen.

Over-All Interference Pressure Distributions Due to Leading-Edge Sources

The over-all interference pressure distributions due to the leading-edge sources are represented by the sums of the pressure distributions of figure 11 plus those of figure 12. The over-all pressure distributions for four spanwise stations are shown in figure 13. This figure brings out a number of significant facts. For points very near the leading edge of the wing-body juncture, the body is effectively an infinite perpendicular reflection plane. Thus, the interference pressure coefficient here is $0.52(t/c)$, just as it is at the root chord of the wing alone for either of the leading-edge sources. If the body were an infinite perpendicular reflection plane, the interference pressure coefficient for all points of the wing-body juncture would be $0.52(t/c)$. However, because the body is curved and is not a perfect reflection plane, the pressure coefficient decreases rapidly to a much lower value a short distance behind the leading edge of the wing-body juncture.

The over-all interference pressure distributions due to the leading-edge sources show increasing positive pressures over the rear part of the wing on the inboard sections and over most of the wing on the outboard sections because of the influence of the opposite half-wing of the combination. The region of influence of one half-wing of the wing-body configuration on the body and the other half-wing can be determined from the following considerations. Consider the leading edge of the wing-body juncture of the left half-wing as a source of pressure disturbances which radiate in all directions to the left within the Mach cone from the source. A pressure disturbance will start to travel in a vertical plane along the intersection of the Mach cone with the body at 45° to the wing-body juncture. After this disturbance has traveled a short distance up the side of the body to a new position P, it can be thought of as the source of a number of secondary disturbances which radiate in all directions within the Mach cone from point P to the left of the plane tangent to the body at point P. The secondary disturbance traveling along the intersection of the Mach cone from P with the body will travel in a direction which is 45° to the element of the cylindrical body through P. The forward boundary of the region of influence of the left half-wing on the body thus intersects the elements of the cylinder at 45°, and would be a straight 45° line if the cylindrical surface of the body were unrolled.

From the knowledge of the position of the forward boundary of the region of influence of the left half-wing on the body, the forward boundary of the region of influence of the left half-wing

on the right half-wing may be determined. From the foregoing paragraph, it is apparent that the effect of the disturbances starting at the leading edge of the left wing-body juncture must travel a distance $\pi(d/2)$ downstream before it can reach the right wing-body juncture. For the present example the effect reaches the right wing-body juncture at about the 78-percent chord, and this position corresponds to the starting point of the forward boundary of the region of influence of the left half-wing on the right half-wing. It might be surmised that this boundary is the Mach line on the right half-wing which starts at the 78-percent-chord position of the right wing-body juncture. However, this is not the case. Consider secondary disturbances from points on the right-hand side of the body. It is apparent that some of these secondary disturbances can reach the right half-wing along straight paths from their respective sources. When account is taken of this effect, it can be shown that the forward boundary of the region of influence of the left half-wing on the right half-wing actually lies in front of the Mach line from the 78-percent-chord position of the right wing-body juncture. The coordinates of the forward boundary are given by the equation

$$\xi = \frac{d}{2}\left[\pi + 2\frac{\sqrt{\eta(\eta+d)}}{d} - \cos^{-1}\left(\frac{d}{2\eta+d}\right)\right] \tag{24}$$

The ξ distance is measured positive downstream from the leading edge of the wing-body juncture and η is the lateral distance from the wing-body juncture. It is apparent that the forward boundary asymptotically approaches a Mach line.

The forward boundary of the region of influence of the left half-wing on the right half-wing, shown in figure 13, is in close agreement with the start of a region of rising positive pressure except near the wing-body juncture. The region of rising positive pressure is a consequence of the positive pressure field of the left leading-edge source passing around the body. If the present analysis had been rigorous to the first order, the region of positive rising pressure would probably have started as a cusp at the forward boundary. The slight discrepancy noted at the wing-body juncture is due to the approximations of the present method.

It is apparent from the foregoing discussion of the over-all interference pressure distributions due to the leading-edge sources

that no cusps should arise in these pressure distributions in front of the forward boundary of the region of influence at the opposite half-wing. The cusps in front of this boundary, shown in figure 13, would have been identically canceled if a precise first-order method rather than an approximate first-order method had been used to obtain the pressure distribution due to cancellation of the finite velocities normal to the body. For these reasons the cusps in question have been faired as shown by the dashed lines in figure 13. The effect of fairing the first cusps near the Mach line of the leading edge is small. However, the fairing of the second and third cusps has an appreciable influence on the pressure distributions and was performed as follows: The fairing started at the second cusp as a continuation of the pressure distribution in front of this cusp and joined the pressure distribution on the tangent direction behind the third cusp. The effect of this fairing on the interference pressure drag is considered in the next section.

Interference Pressure Drag of Half-Wings

As previously pointed out, the interference pressure drag is equal to the drag of the wing in combination minus that of the wing alone for the configurations considered in this report. The wing alone is taken to be the two half-wings joined together. The pressure drag of the wing alone is considered before determining the interference pressure drag. The spanwise distribution of pressure drag for the wing alone is shown in figure 14. This figure is based on results of reference 9 and was obtained using the line pressure-source theory of R. T. Jones (reference 5). The pressure drag on the given half-wing due to its own pressure field accounts for most of the wing-alone drag. In fact, for a 10-percent-thick wing the pressure drag coefficient is 0.0086, of which 0.0064 is due to the pressure fields of the half-wings acting on themselves, while 0.0022 is due to the pressure fields of the half-wings acting on the opposite half-wings. The effect of the wing tips on the spanwise distribution of the pressure drag has not been included in the figure, since, as previously mentioned, the presence of the tip changes only the distribution of the pressure drag within the Mach cones from the leading edge of the tips and does not change the over-all wing drag (references 8 and 9).

The spanwise variation of the pressure drag of the half-wing associated with the over-all interference pressure distribution can easily be determined from the over-all interference pressure distribution due to the leading-edge sources (fig. 13). Denoting the average values of $P/(t/c)$ for any spanwise station over the

chordwise interval from $-1.0c$ to $-0.5c$ as n_1, from $-0.5c$ to 0 as n_2, from 0 to $0.5c$ as n_3, and from $0.5c$ to $1.0c$ as n_4, the section drag coefficient due to the over-all interference pressure distribution for the leading-edge sources is $(n_3-n_4)\ (t/c)^2$. The section drag coefficient for the midchord-line sinks is $-2(n_2-n_3)\ (t/c)^2$ and that for the trailing-edge sources is $(n_1-n_2)\ (t/c)^2$. Thus the resultant section drag coefficient is

$$c_d = (n_1-3n_2+3n_3-n_4)\left(\frac{t}{c}\right)^2 \qquad (25)$$

Equation (25) is valid only for the present wing, which has a symmetrical double-wedge section with the maximum thickness at the midchord.

With the aid of equation (25), the spanwise distribution of the pressure drag has been determined from the over-all interference pressure distributions of figure 13, both for the faired and the unfaired curves. (See fig. 15.) Smooth curves have been drawn through the calculated points shown in figure 15 as squares for the unfaired condition and as circles for the faired condition. The spanwise distribution of the pressure drag for the two cases is considerably different. The importance of the difference can perhaps best be assessed by a comparison of the drag coefficients for the wing in combination for the two conditions. The drag coefficient of either half-wing, neglecting interference effects, is represented by the upper curve of figure 14, and, for a 10-percent-thick wing, this drag coefficient is 0.0064. The drag coefficient of the wing alone is obtained by adding the effect of the opposite half-wing and is 0.0086 for the same wing thickness. When the drag coefficients represented by the two curves of figure 15 are added to 0.0064, the resulting drag coefficient for the wing in combination, including interference effects, is 0.0075 for the unfaired case and 0.0060 for the faired case. Thus, the drag of the wing in combination is 87 percent of the drag of the wing alone for the over-all interference pressure distributions with the cusps, and 70 percent without the cusps. In either case, the effect of interference is favorable. It is probable that the 30-percent reduction in drag coefficient represents a closer approximation to the first-order answer for the same reasons that it is believed the faired over-all interference pressure distributions represent a closer approximation to the first-order pressure distributions than do the unfaired ones. It should be noted that the foregoing results apply only to the wing-body configuration of the example for $M_0=\sqrt{2}$, and it is conceivable that for other configurations and Mach numbers the effect of interference may be considerably different.

The results considered so far have been for distances of the origins of the image sinks from their respective wing–body junctures of 0.05d. The results obtained by the present method should not vary much with small changes in the image–sink distances from this value. The results of calculations using a 9–ring scheme and image–sink distances of 0.1d substantiate this statement. The spanwise distribution of the pressure drag determined from these calculations, using the faired curves, are shown in figure 15 as triangles, and the distribution is in good accord with that for the 18–ring scheme with image–sink distances of 0.05d.

When the effect on the wing pressures of the pressure field of the portion of the body in front of the region of influence of the wing is neglected, the pressure drag of the wing–body configuration is less than the sum of the pressure drags of the body alone and the wing alone. For a position of the wing well back on the body, the effect of the nose should be small; but for a position of the wing near the nose, the effect of the nose on the wing may be greater than the other interference effects. This appears to be a worthwhile point to investigate, especially since it is amenable to simple analysis. Another effect which may modify the pressure drag of the wing–body combination is the effect that the interference pressure field may have on the boundary layer of the combination.

The analysis has been for $M_0 = \sqrt{2}$. However, this does not limit its applicability since any wing–body configuration at a Mach number other than $\sqrt{2}$ has an equivalent wing–body configuration at $M_0 = \sqrt{2}$. To determine the interference pressures on a wing–body combination at a Mach number other than $\sqrt{2}$, multiply the longitudinal dimensions of the wing–body configuration by the factor $1/\sqrt{M_0^2-1}$ to give an equivalent wing–body combination at $M_0 = \sqrt{2}$. Solve for the interference pressures of the equivalent wing–body combination by the method of this report. Then the pressure coefficient at a point on the actual wing–body configuration at a Mach number other than $\sqrt{2}$ is equal to the pressure coefficient at the corresponding point of the equivalent wing–body configuration divided by $\sqrt{M_0^2-1}$.

Ames Aeronautical Laboratory,
National Advisory Committee for Aeronautics,
Moffett Field, Calif.

REFERENCES

1. Jones, Robert T.: Properties of Low-Aspect-Ratio Pointed Wings at Speeds Below and Above the Speed of Sound. NACA TN No. 1032, 1946.

2. Spreiter, John R.: Aerodynamic Properties of Slender Wing-Body Combinations at Subsonic, Transonic, and Supersonic Speeds. NACA TN No. 1662, 1948.

3. Browne, S. H., Friedman, L., and Hodes, I.: A Wing-Body Problem in a Supersonic Conical Flow. Jour. Aero. Sci., vol. 15, no. 8, Aug. 1948, pp. 443-452.

4. Ferrari, Carlo: Interference Between Wing and Body at Supersonic Speeds - Theory and Numerical Application. Jour. Aero. Sci., vol. 15, no. 6, June, 1948, pp. 317-336.

5. Jones, Robert T.: Thin Oblique Airfoils at Supersonic Speed. NACA TN No. 1107, 1946.

6. Puckett, Allen E.: Supersonic Wave Drag of Thin Airfoils. Jour. Aero. Sci., vol. 13, no. 9, Sept. 1946, pp. 475-484.

7. von Kármán, Theodore, and Moore, Norton B.: Resistance of Slender Bodies Moving with Supersonic Velocities, with Special Reference to Projectiles. Trans. A.S.M.E., vol. 54, no. 23, Dec. 15, 1932, pp 303-310.

8. Nielsen, Jack N.: Effect of Aspect Ratio and Taper on the Pressure Drag at Supersonic Speeds of Unswept Wings at Zero Lift. NACA TN No. 1487, 1947.

9. Margolis, Kenneth: Supersonic Wave Drag of Sweptback Tapered Wings at Zero Lift. NACA TN No. 1448, 1947.

TABLE I

FACTOR k FOR DETERMINING THE AVERAGE NORMAL VELOCITY INDUCED THROUGH THE CONTROL AREAS BY THE RECTANGULAR WEDGE COINCIDING WITH SIDE A OF THE OCTAGONAL PRISM AND OF WHICH THE REGION OF INFLUENCE ON THE BODY BEGINS AT $\xi = 0$

Strip					Ring
E	D	C	B	A	
0	0	0	0.069	0.813	I
0	0	0	.189	.887	II
0	0	.062	.273	.861	III
0	.030	.224	.255	.851	IV
.240	.295	.218	.230	.845	V
.242	.210	.165	.223	.840	VI
.180	.165	.153	.218	.835	VII
.160	.152	.146	.214	.833	VIII
.145	.144	.142	.211	.832	IX
.139	.139	.139	.209	.832	X
.136	.135	.137	.208	.832	XI
.134	.134	.135	.207	.832	XII
.133	.132	.134	.206	.834	XIII
.131	.131	.133	.206	.836	XIV
.130	.130	.132	.206	.838	XV
.130	.130	.132	.206	.840	XVI
.130	.130	.132	.206	.841	XVII
.130	.130	.132	.206	.842	XVIII

TABLE II

FACTORS FOR ADJUSTING THE AVERAGE FINITE NORMAL VELOCITY AT VARIOUS CONTROL AREAS DUE TO OCTAGONAL PRISM OF RECTANGULAR WEDGES WITH REGION OF INFLUENCE ON BODY BEGINNING AT $\xi = 0$

Strip			Ring
C	B	A	
0 .138 .813	0.069 .813 .069	k_1=0.813 k_2= .138 k_3=0	I
0 .378 .887	.189 .887 .189	0.887 .378 0	II
.124 .546 .861	.273 .985 .273	.861 .546 .124	III
.448 .570 .851	.285 1.299 .285	.851 .570 .448	IV
.436 1.050 1.085	.525 1.521 .525	1.085 1.050 .436	V
.330 .866 1.082	.433 1.412 .433	1.082 .866 .330	VI
.306 .766 1.015	.383 1.321 .383	1.015 .766 .306	VII
.292 .732 .993	.366 1.285 .366	.993 .732 .292	VIII
.284 .710 .977	.355 1.261 .355	.977 .710 .284	IX

Strip			Ring
C	B	A	
0.278 .696 .971	0.348 1.249 .348	0.971 .696 .278	X
.274 .686 .968	.343 1.242 .343	.968 .686 .274	XI
.270 .682 .966	.341 1.236 .341	.966 .682 .270	XII
.268 .676 .967	.338 1.235 .338	.967 .676 .268	XIII
.266 .674 .967	.337 1.233 .337	.967 .674 .266	XIV
.264 .672 .968	.336 1.232 .336	.968 .672 .264	XV
.264 .672 .970	.336 1.234 .336	.970 .672 .264	XVI
.264 .672 .971	.336 1.235 .336	.971 .672 .264	XVII
.264 .672 .972	.336 1.236 .336	.972 .672 .264	XVIII

TABLE III

RATIOS OF AVERAGE FINITE NORMAL VELOCITY TO FREE-STREAM VELOCITY $\bar{v}_n/V_o$ THROUGH CONTROL AREAS AFTER CANCELING INFINITE SIDE-WASH OF LEADING-EDGE SOURCES FOR 10-PERCENT-THICK WING

Strip			Ring
C	B	A	
0	0.	0.001	I
0	.0015	−.0100	II
.0010	.0065	−.0200	III
.0080	.0040	−.0300	IV
.0190	.0070	−.0350	V
.0210	.0120	−.0300	VI
.0240	.0110	−.0350	VII
.0275	.0130	−.0390	VIII
.0300	.0130	−.0390	IX
.0315	.0140	−.0410	X
.0325	.0140	−.0410	XI
.0340	.0140	−.0420	XII
.0340	.0150	−.0440	XIII
.0350	.0150	−.0450	XIV
.0360	.0150	−.0460	XV
.0370	.0150	−.0460	XVI
.0380	.0150	−.0460	XVII
.0390	.0150	−.0470	XVIII

TABLE IV

SLOPE OF RECTANGULAR WEDGES CANCELING
AVERAGE FINITE NORMAL VELOCITIES

$\left(\frac{dz}{dx}\right)_C$	$\left(\frac{dz}{dx}\right)_B$	$\left(\frac{dz}{dx}\right)_A$	Ring
−0.00002	0.00011	−0.00125	I
.00046	−.00290	.01411	II
.00131	−.00917	.01336	III
−.00705	−.00009	.01479	IV
−.01803	−.00312	.00783	V
−.00499	−.00453	−.00601	VI
−.00311	.00295	.01513	VII
−.00392	−.00297	.00666	VIII
.00539	.00442	.00063	IX
−.00619	−.00040	.00641	X
−.00707	−.00585	−.00721	XI
.00292	.00090	.00127	XII
−.00484	−.00212	.00418	XIII
.00475	.00269	.00344	XIV
.00293	.00445	.00484	XV
−.00832	−.00457	−.00279	XVI
−.00025	−.00018	−.00243	XVII
−.00468	−.00176	−.01358	XVIII

TABLE V

FACTORS FOR DETERMINING THE WING PRESSURE COEFFICIENTS DUE TO THE FIRST SET OF RECTANGULAR WEDGES

$\eta/s = 0$		$\eta/s = 0.05$		$\eta/s = 0.125$	
Position	Factor	Position	Factor	Position	Factor
0.018c	$C_1 = 0$ $C_2 = 0$ $C_3 = 0$	0.082c	$C_1 = 0.7788$ $C_2 = 1.0536$ $C_3 = 0$	0.026c	$C_1 = 0.6026$ $C_2 = 1.0204$ $C_3 = 0$
.118c	1.0522 1.0000 0	.182c	0.4476 1.4300 0	.126c	0.3730 1.3408 0
.218c	.5324 1.5028 0	.282c	.3194 .7780 1.0480	.226c	.2764 .6612 .9824
.318c	.3628 .9024 1.0916	.382c	.2496 1.7356 .8508	.326c	.2212 1.5696 .7372
.418c	.2760 1.8796 .9660	.482c	.6858 1.2024 .5396	.426c	.6342 1.0996 .4896
.518c	.7274 1.2912 .5832	.582c	.4462 .8613 .4168	.526c	.4152 .7980 .3840
.618c	.4714 .9144 .4436	.682c	.3549 .6990 .3443	.626c	.3322 .6528 .3204
.718c	.3730 .7368 .3636	.782c	.3000 .5952 .2953	.726c	.2824 .5592 .2768
.818c	.3138 .6240 .3100	.882c	.2616 .5212 .2594	.826c	.2474 .4920 .2444
.918c	.2730 .5440 .2712	.982c	.2331 .4648 .2316	.926c	.2210 .4404 .2196
1.018c	.2422 .4832 .2412	- - -	- - -	1.026c	.2006 .4008 .1996

TABLE V.- CONTINUED

$\eta/s = 0.25$		$\eta/s = 0.50$		$\eta/s = 0.75$		$\eta/s = 1.00$	
Position	Factor	Position	Factor	Position	Factor	Position	Factor
−0.065c	$C_1 = 0.4670$ $C_2 = .9416$ $C_3 = 0$	−0.248c	$C_1 = 0.3482$ $C_2 = .8168$ $C_3 = 0$	−0.431c	$C_1 = 0.2900$ $C_2 = .7280$ $C_3 = 0$	−0.614c	$C_1 = 0.2536$ $C_2 = .6648$ $C_3 = 0$
.035c	0.3036 .9128 .3431	−.148c	0.2346 .6432 .4076	−.331c	0.1981 .5284 .3902	−.514c	0.1746 .4584 .3663
.135c	.2322 .5468 .8916	−.048c	.1840 .4280 .7648	−.231c	.1571 .3639 .6796	−.414c	.1394 .3215 .6180
.235c	.1898 1.3772 .6204	.052c	.1536 1.1456 .4928	−.131c	.1324 .9678 .4216	−.314c	.1182 .9027 .3742
.335c	.5701 .9750 .4300	.152c	.4852 .8144 .3564	−.031c	.4299 .7327 .3108	−.214c	.3911 .6435 .2792
.435c	.3759 .7174 .3434	.252c	.3222 .6100 .2900	.069c	.2870 .5455 .2558	−.114c	.2611 .4893 .2312
.535c	.3026 .5923 .2898	.352c	.2616 .5096 .2480	.169c	.2340 .4566 .2204	−.014c	.2136 .4133 .2004
.625c	.2588 .5114 .2525	.452c	.2256 .4436 .2188	.269c	.2026 .3997 .1956	.086c	.1854 .3634 .1782

TABLE V.– CONCLUDED

η/s = 0.25		η/s = 0.50		η/s = 0.75		η/s = 1.00	
Position	Factor	Position	Factor	Position	Factor	Position	Factor
0.735c	0.2280 .4528 .2247	0.552c	0.2002 .3964 .1960	0.369c	0.1804 .3579 .1762	0.186c	0.1656 .3268 .1614
.835c	.2049 .4077 .2027	.652c	.1810 .3592 .1784	.469c	.1639 .3258 .1612	.286c	.1509 .2988 .1481
.935c	.1864 .3715 .1852	.752c	.1654 .3296 .1640	.569c	.1505 .2997 .1487	.386c	.1389 .2759 .1371
1.035c	.1714 .3417 .1705	.852c	.1528 .3052 .1520	.669c	.1395 .2783 .1384	.486c	.1291 .2568 .1278
---	---	.952c	.1422 .2836 .1416	.769c	.1304 .2602 .1294	.586c	.1210 .2409 .1198
---	---	1.052c	.1332 .2660 .1324	.869c	.1225 .2444 .1217	.686c	.1138 .2268 .1132
---	---	---	---	.969c	.1155 .2308 .1150	.786c	.1076 .2146 .1071
---	---	---	---	1.069c	.1094 .2185 .1090	.886c	.1021 .2038 .1016
---	---	---	---	---	---	.986c	.0973 .1940 .0968

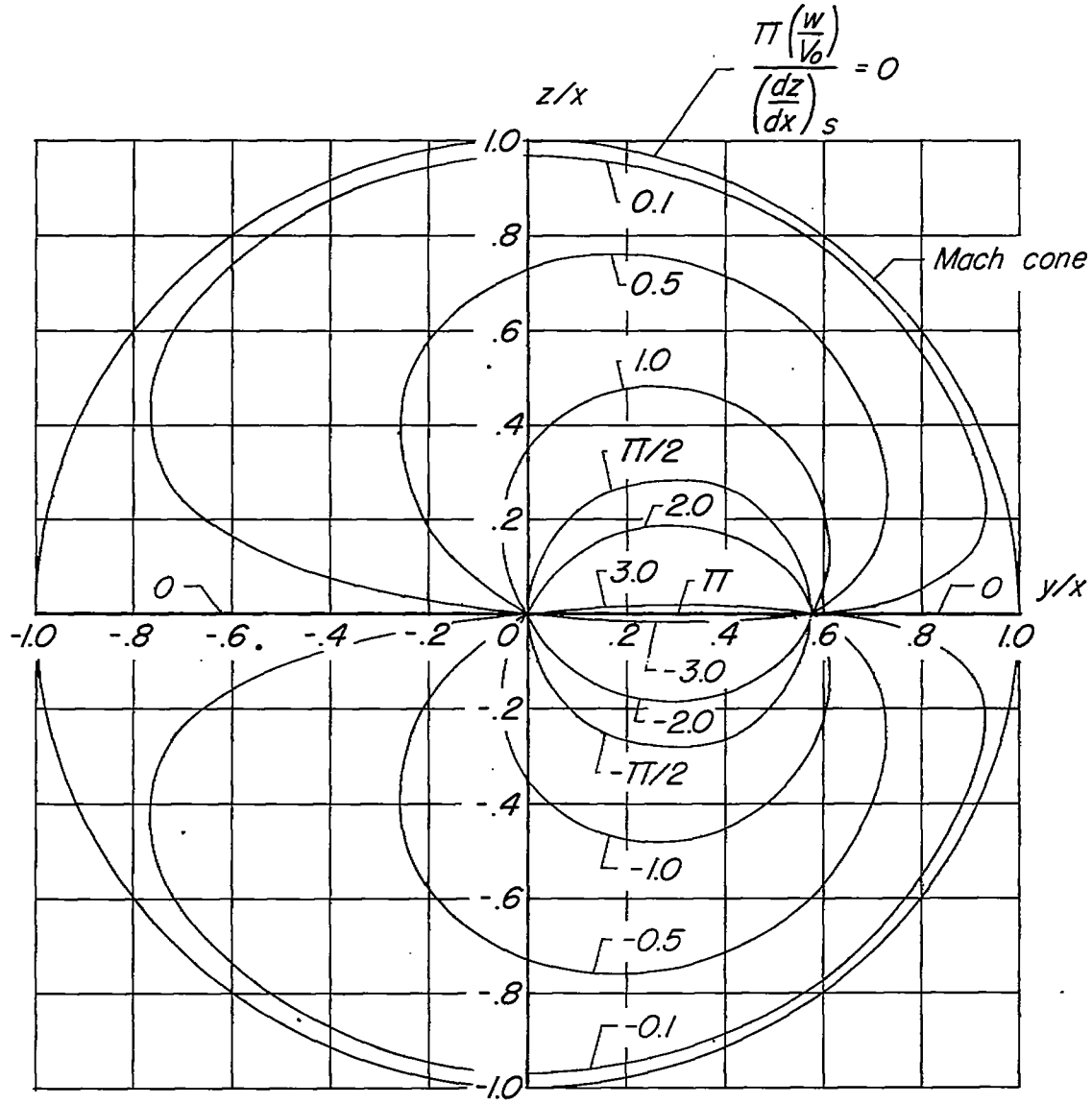

Wedge extends from 0 to 0.577 on y/x axis

Figure 1. - Downwash contours for line pressure source swept back 60°. $M_0 = \sqrt{2}$.

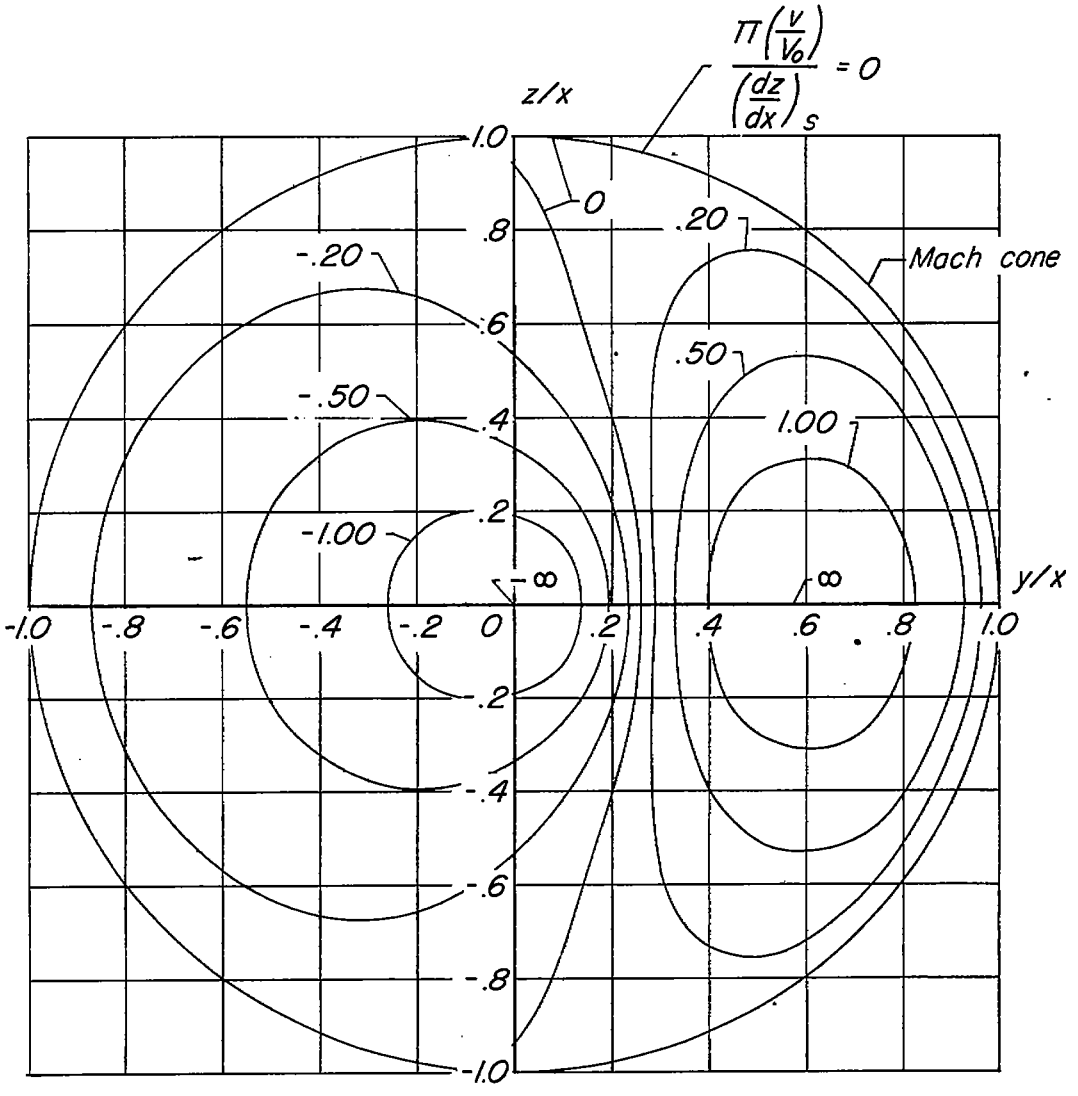

Wedge extends from 0 to 0.577 on y/x axis

Figure 2.- Sidewash contours for line pressure source swept back 60°. $M_0 = \sqrt{2}$.

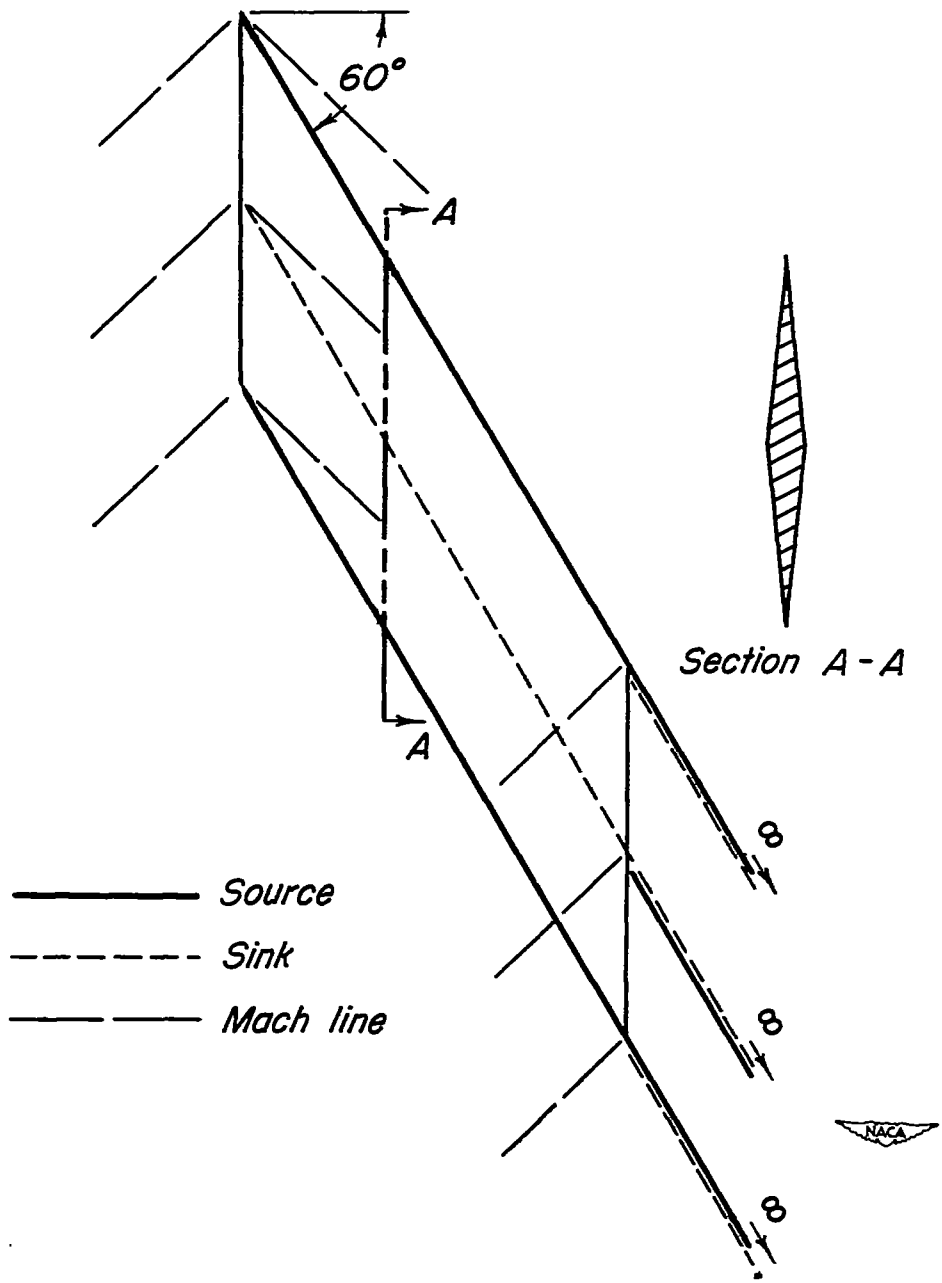

Figure 3. - Source - sink system forming an untapered half - wing swept back at 60° with a symmetrical double - wedge section. $M_o = \sqrt{2}$.

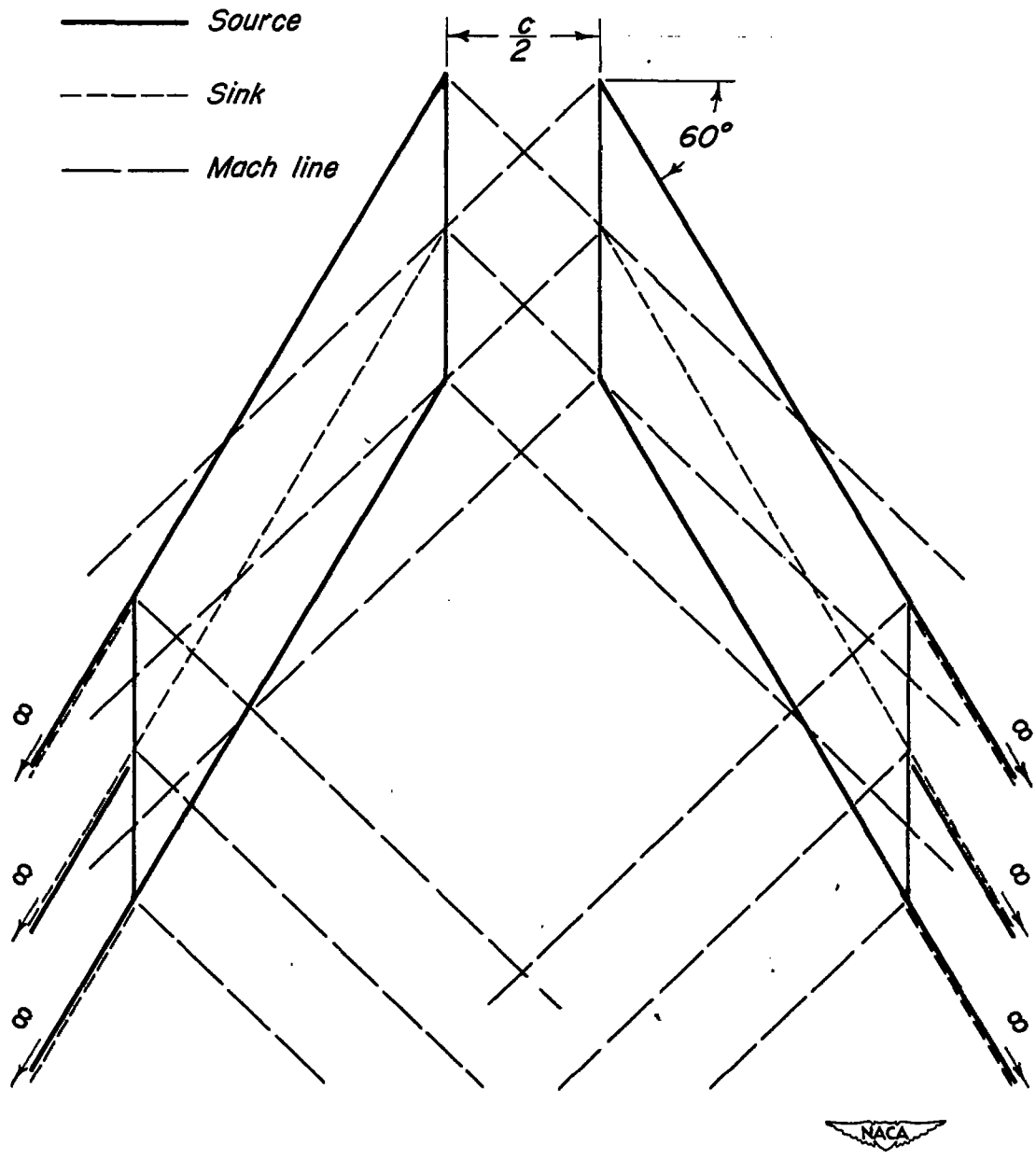

Figure 4.- Interaction between pressure fields of two half-wings separated by half a chord length. $M_o = \sqrt{2}$.

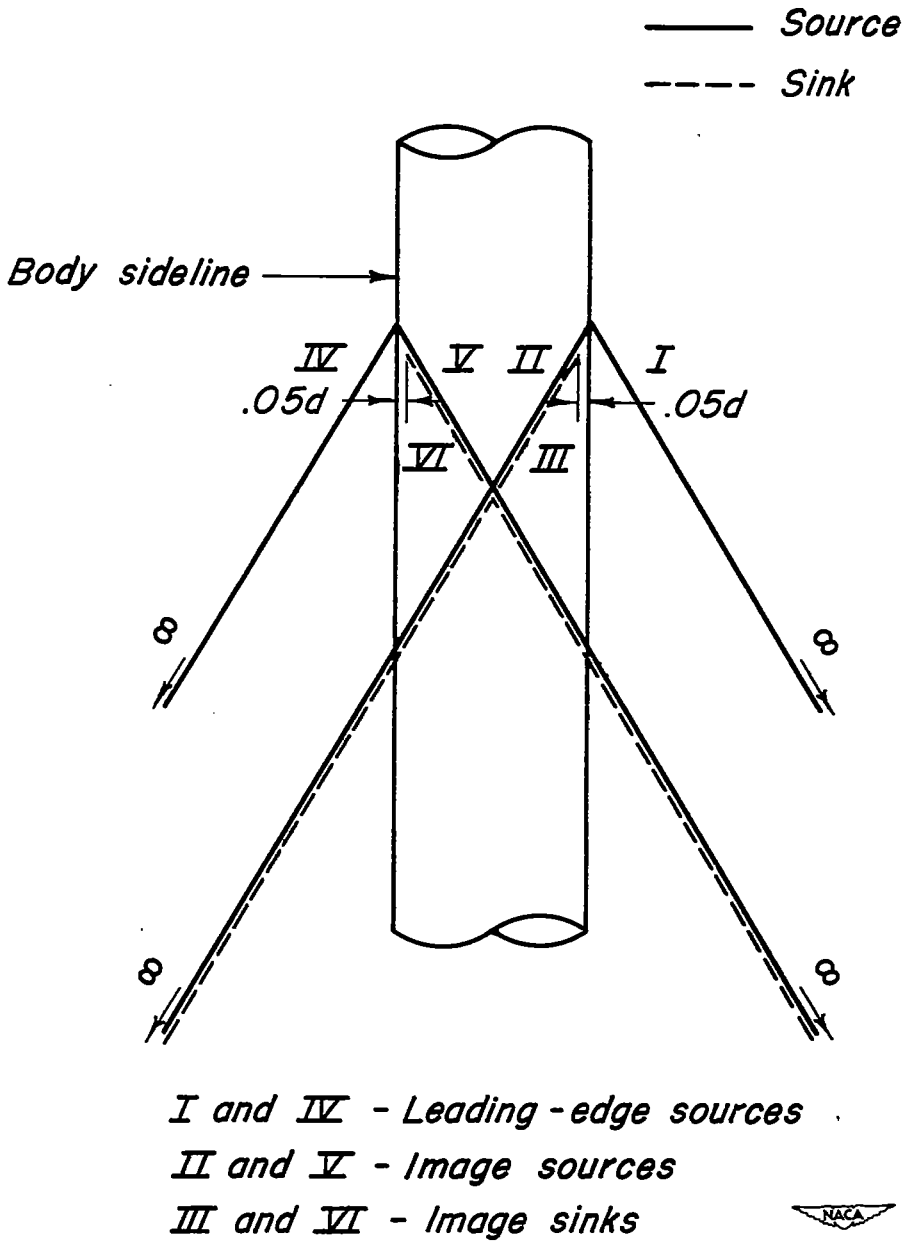

Figure 5.- Source-sink system for reduction of infinite sidewash velocities normal to body due to leading-edge sources.

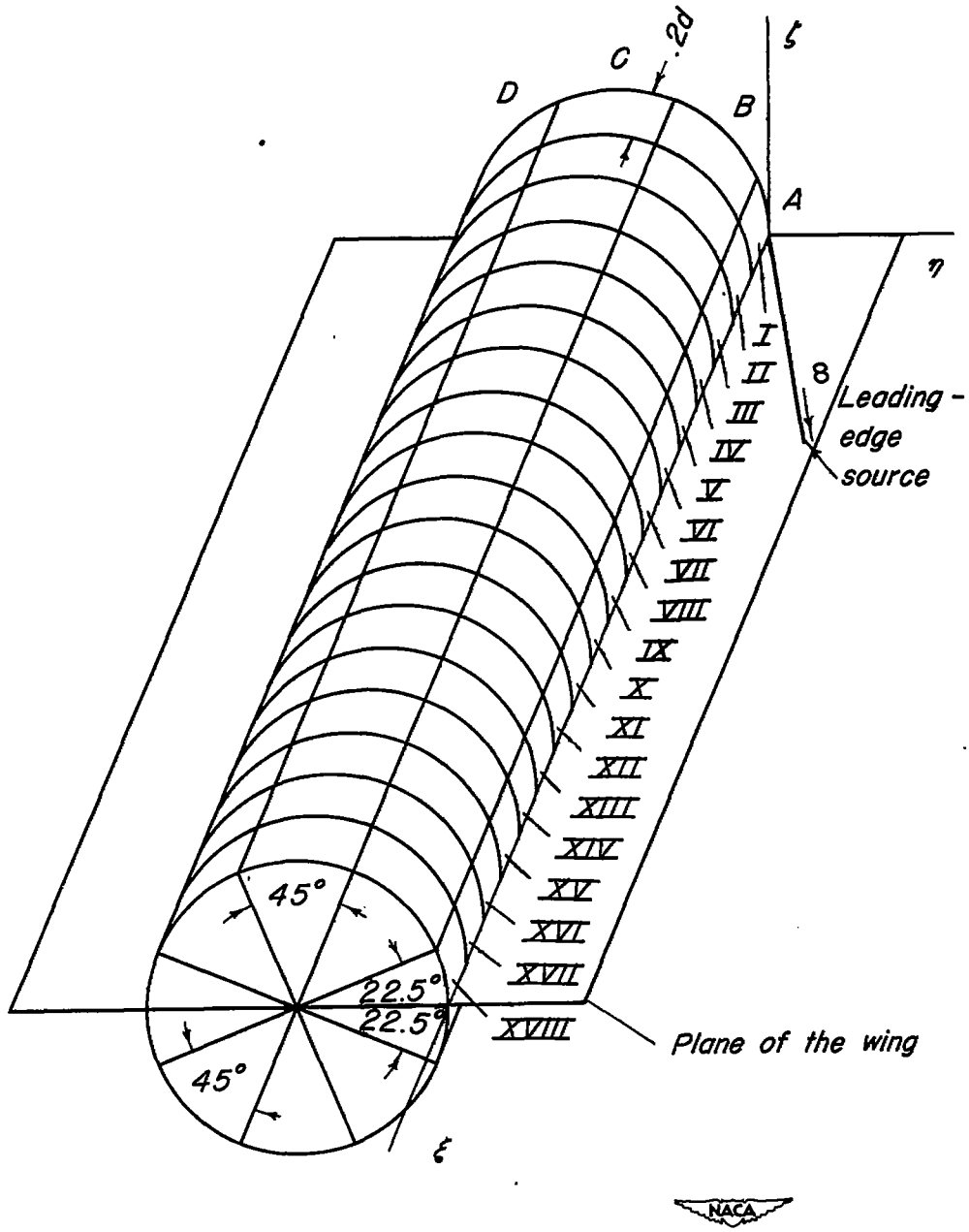

Figure 6 - Control areas used in approximately canceling finite velocities normal to body.

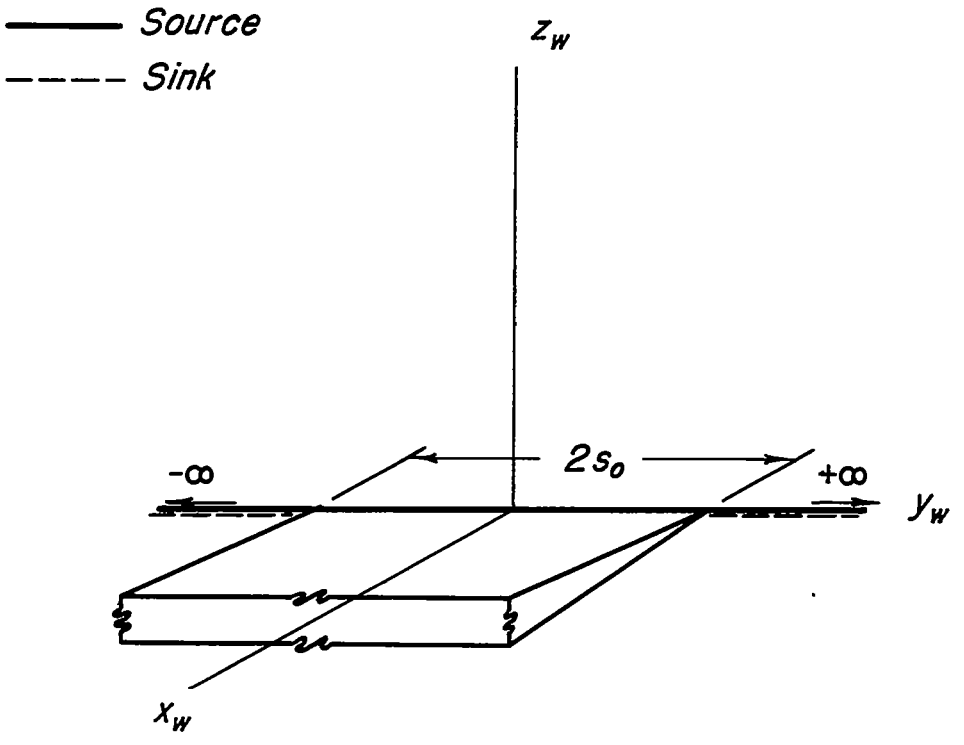

Figure 7. - Source - sink system forming rectangular wedge of infinite chord.

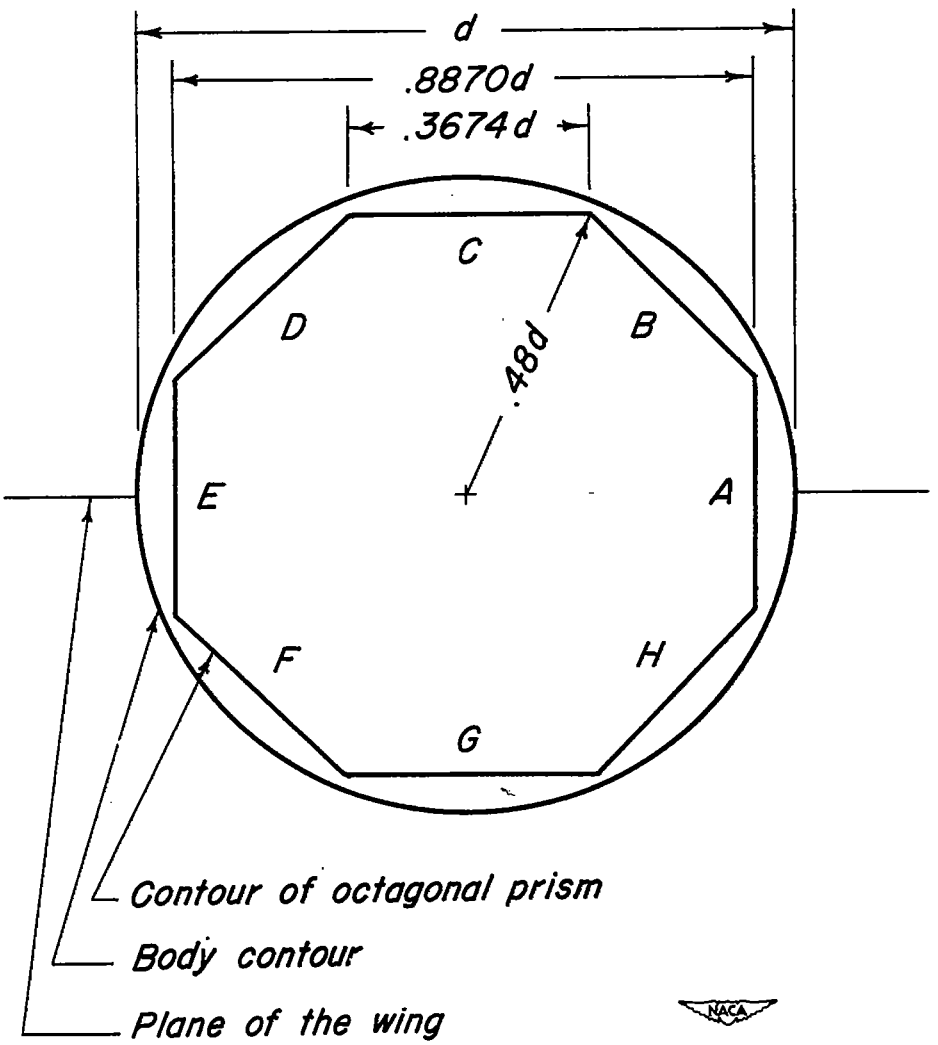

Figure 8. - Cross - sectional view of regular octagonal prism inside of circular body.

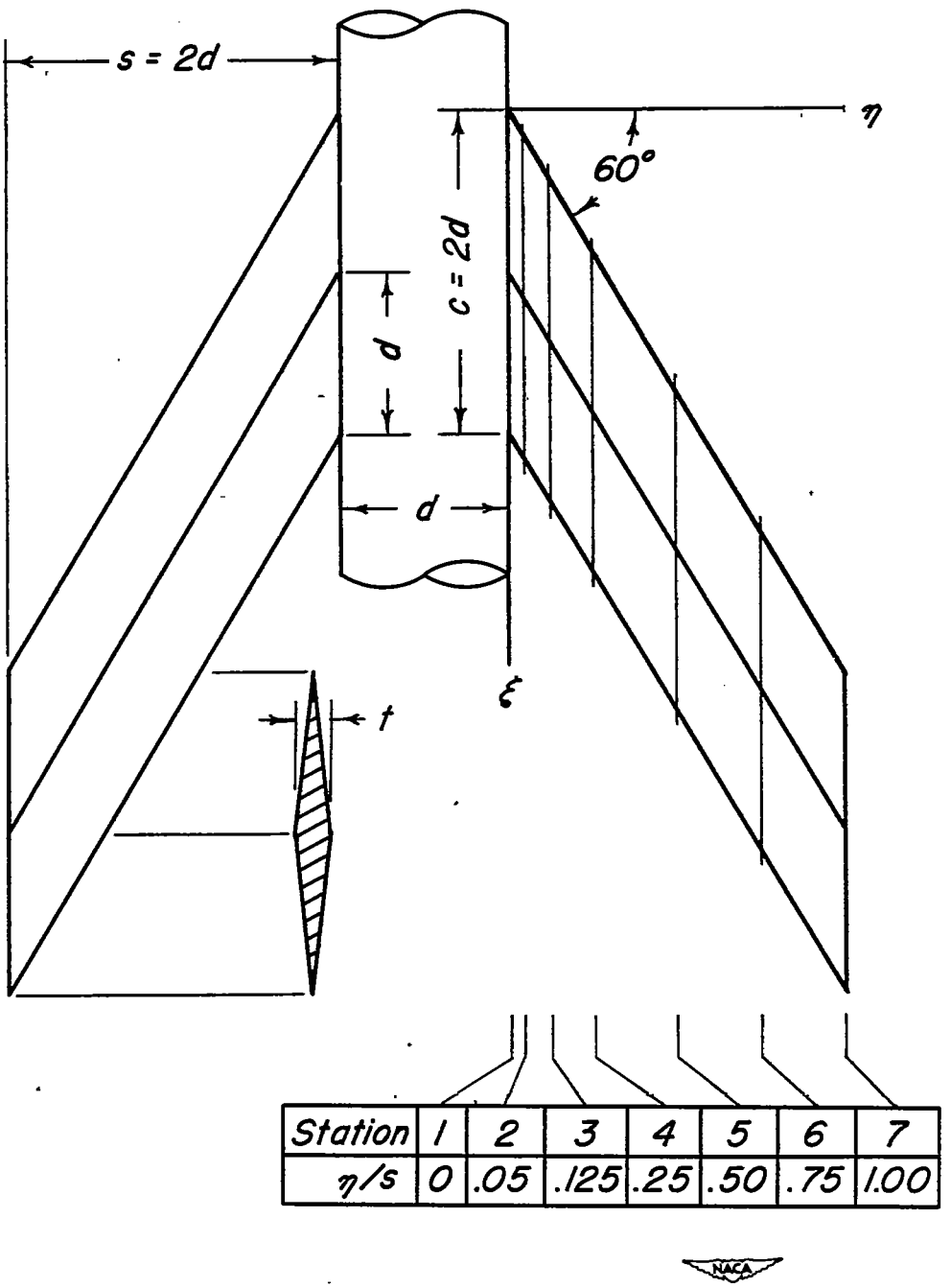

Station	1	2	3	4	5	6	7
η/s	0	.05	.125	.25	.50	.75	1.00

Figure 9.- Dimensions of wing - body configuration used in illustrative example.

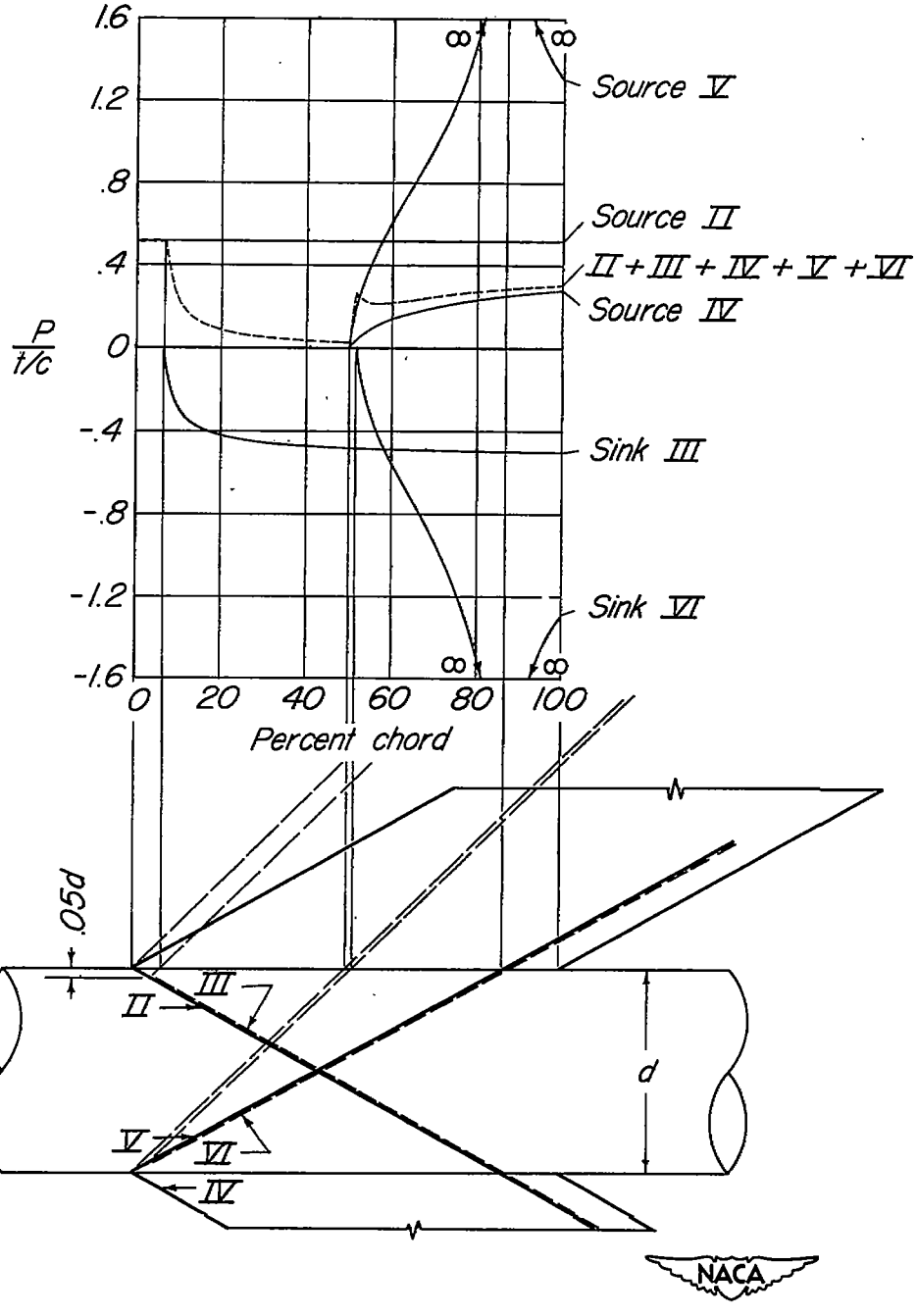

Figure 10. - Pressure distribution at right wing - body juncture due to leading - edge source of left half - wing and due to reduction of infinite sidewash velocities of leading - edge sources. $M_0=\sqrt{2}$.

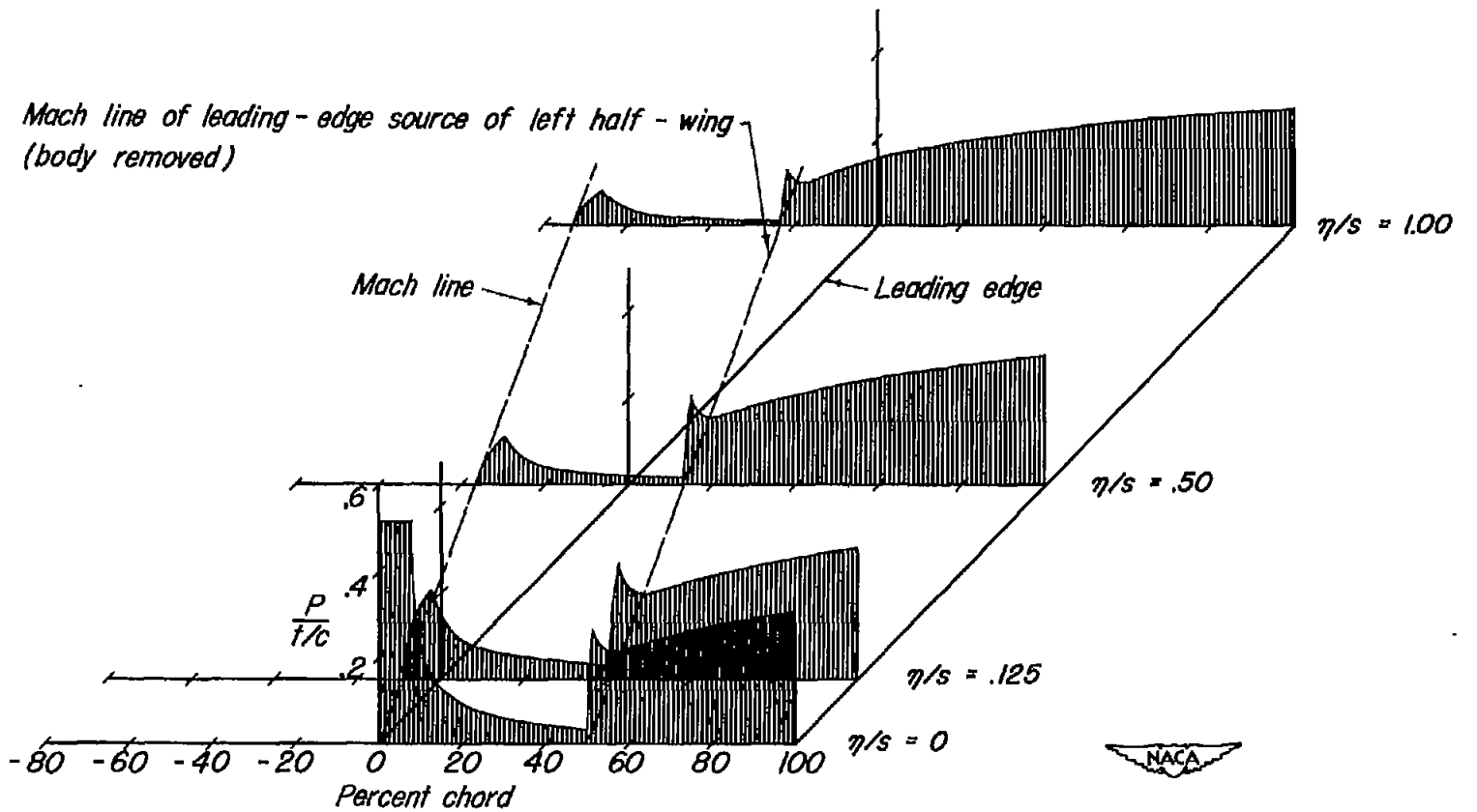

Figure 11. - Spanwise variation of pressure distribution due to leading - edge source of left half - wing and due to reduction of infinite sidewash velocities of leading - edge sources.

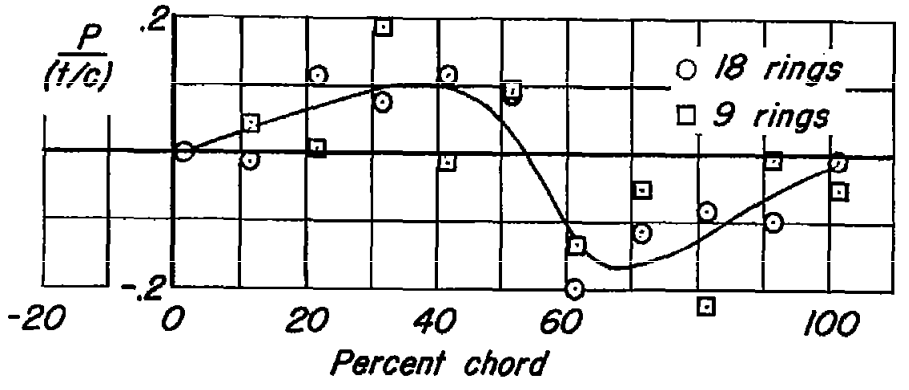

(a) $\eta/s = 0$

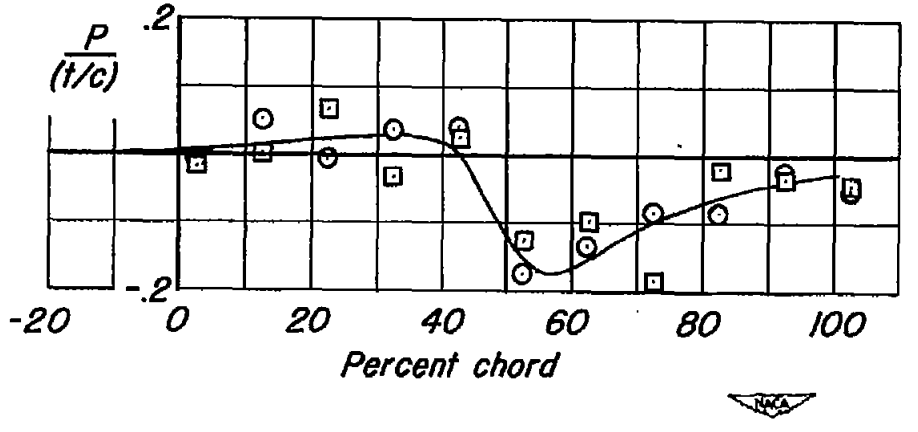

(b) $\eta/s = .125$

Figure 12 - Interference pressure distributions due to approximate cancellation of finite velocities normal to body due to leading - edge sources.

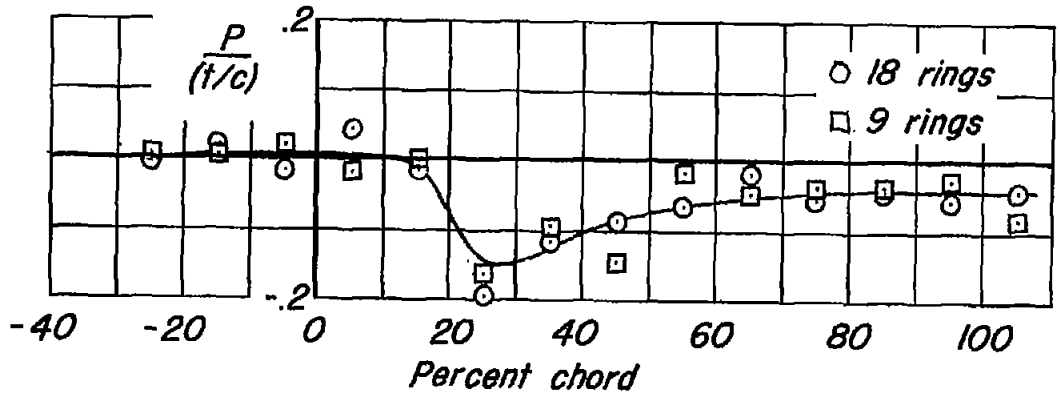

(c) $\eta/s = .50$.

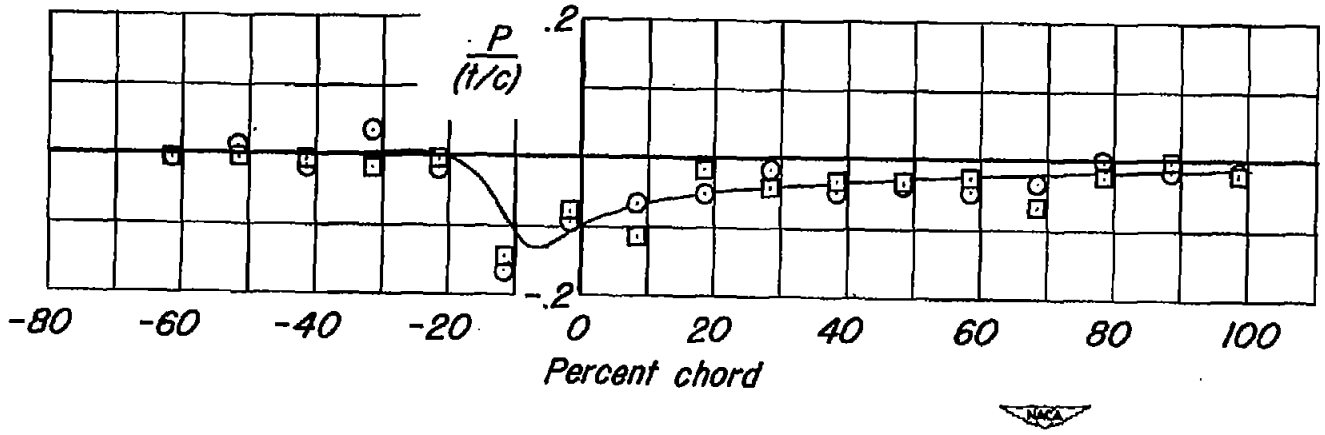

(d) $\eta/s = 1.00$

Figure 12. - Concluded.

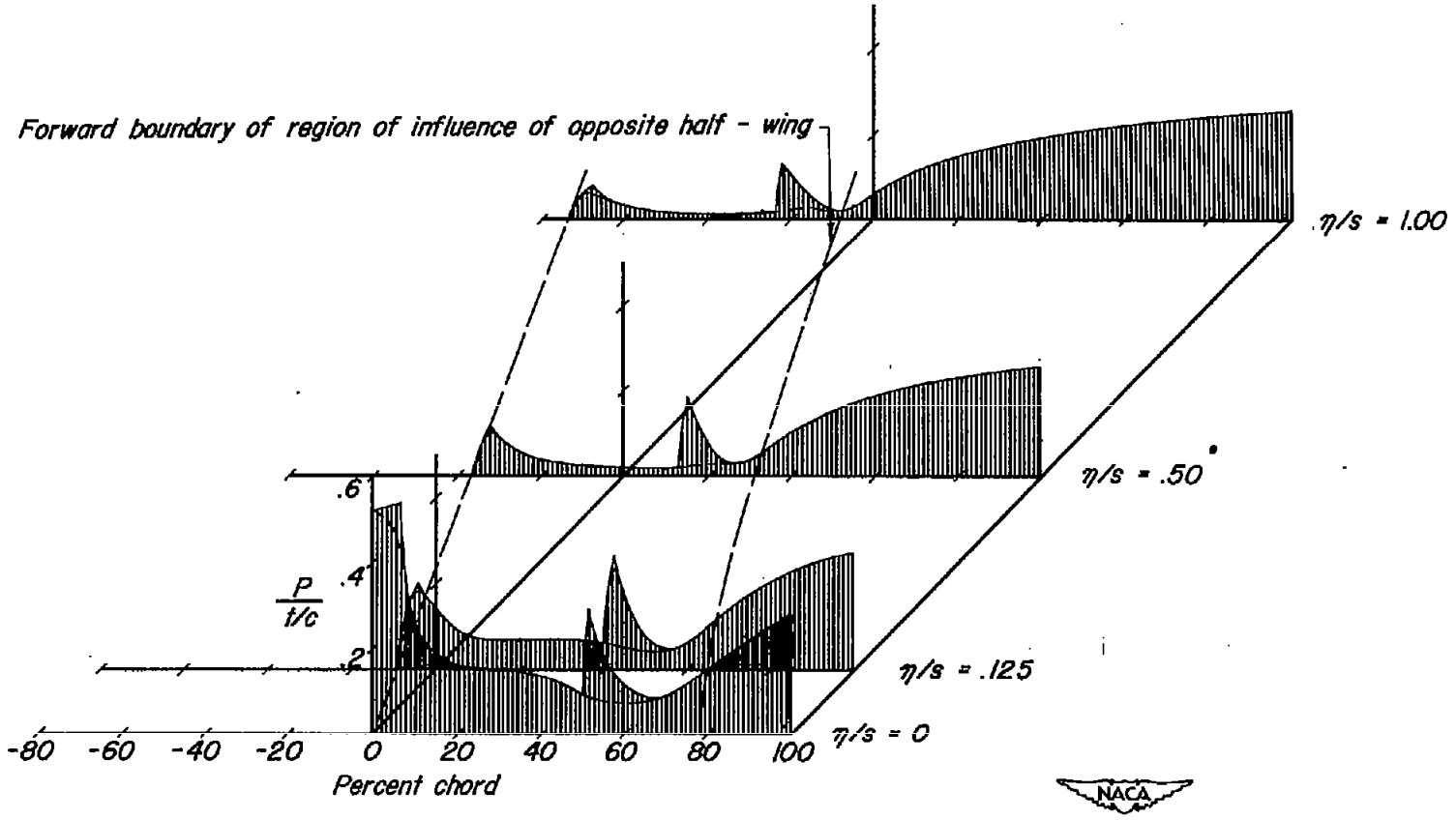

Figure 13.- Over-all interference pressure distributions due to leading-edge sources for wing in combination with body.

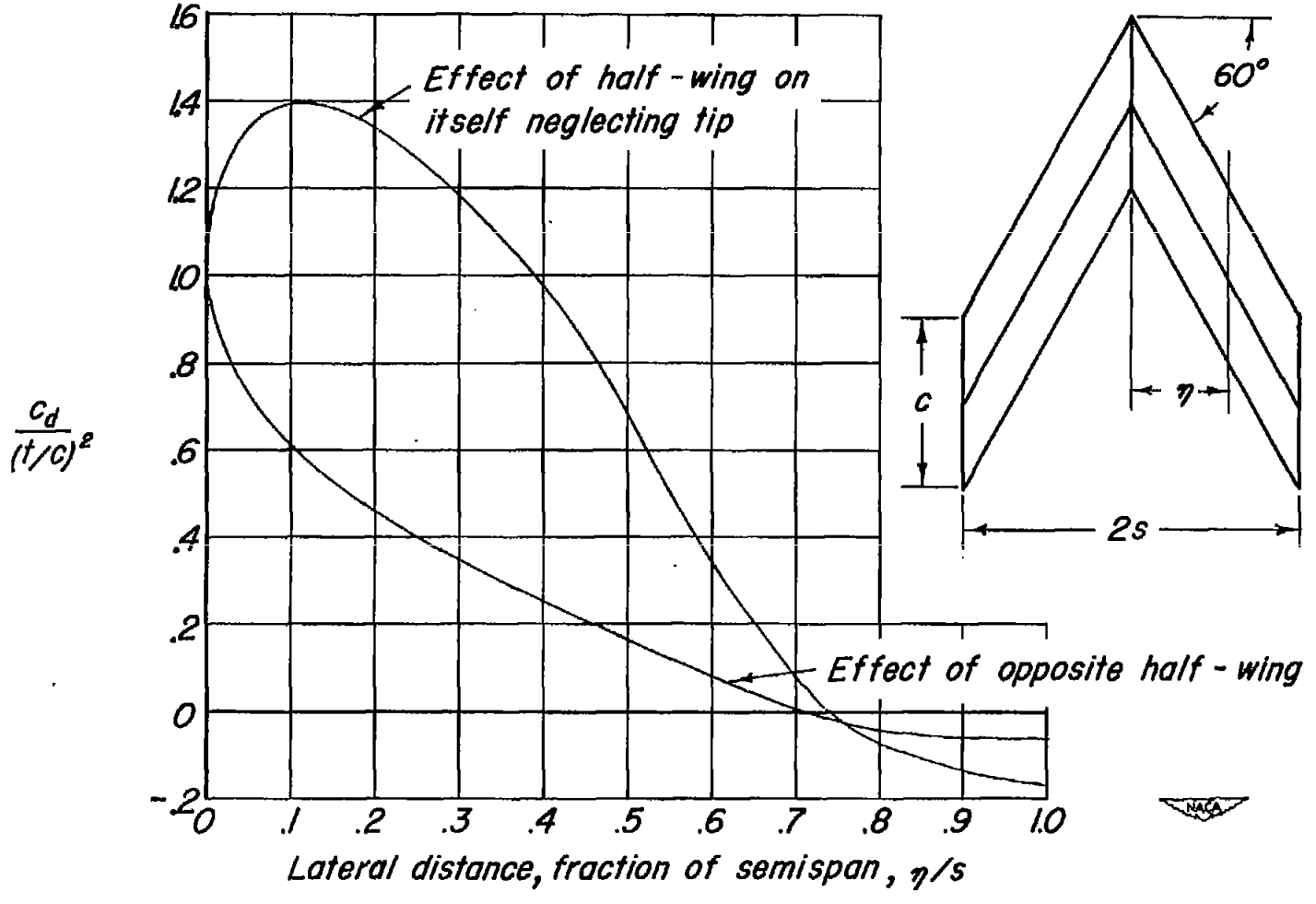

Figure 14.- Spanwise distribution of the pressure drag for either half-wing with half-wings joined at root. $M_e = \sqrt{2}$.

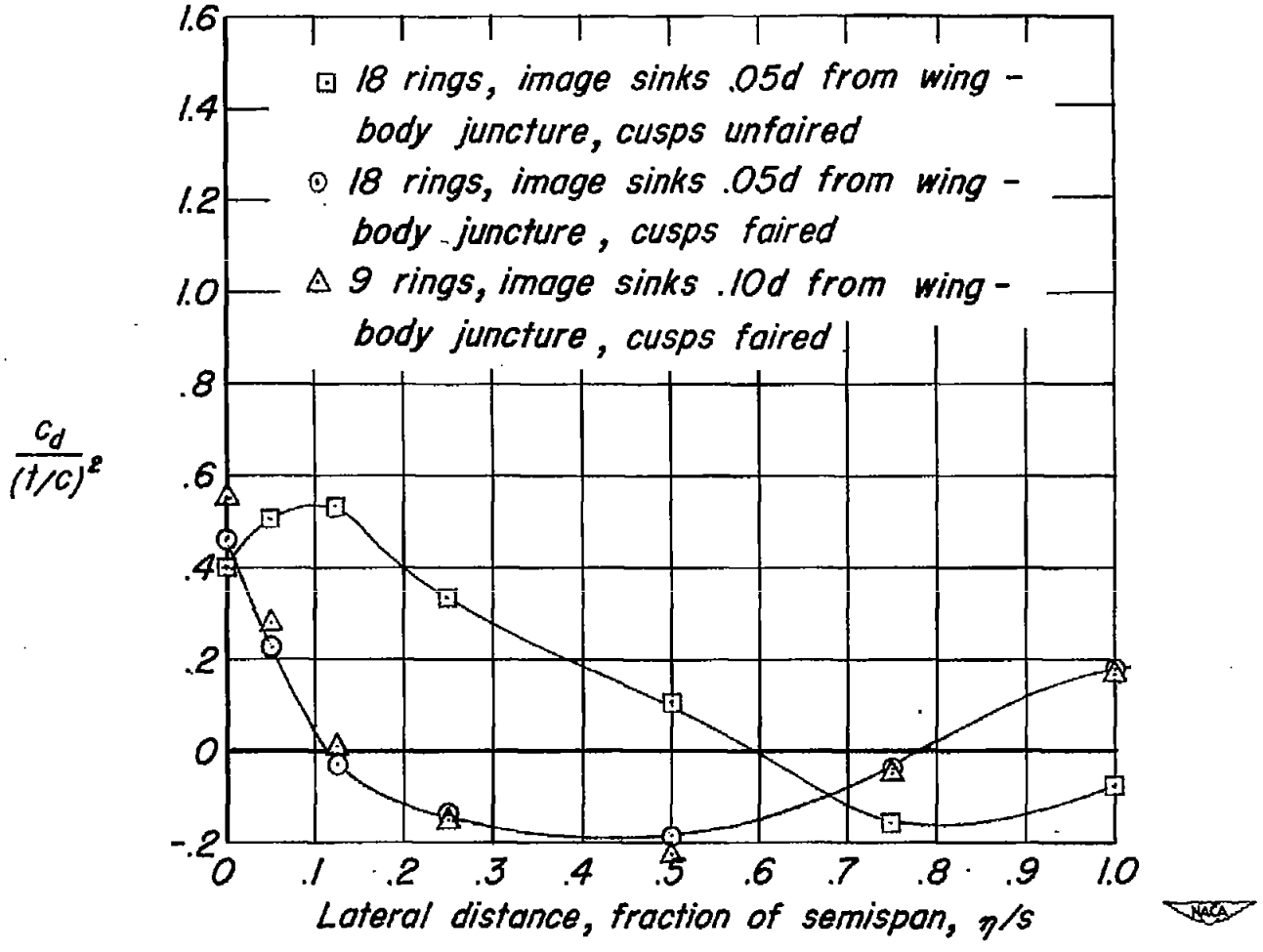

Figure 15.- Spanwise distribution of the pressure drag associated with the over-all interference pressure distribution.

NACA-Langley - 8-5-49 - 375